CHAPTER 7

THE "LEROS" WEAR MACHINE. DESCRIPTION, TEST PROGRAMME and VIBRATION ANALYSIS.

7.1 Introduction

Comparative reviewing of wear test results must be qualified by a knowledge of the type of testing machine used, as even small changes in test conditions can affect the "wear system", as shown in Chapter 4. An in-house, wear machine has been constructed (the **LE**icester **RO**lling-**S**liding wear machine, called LEROS). It was designed both to supplement and to improve on the test programme of the modified Amsler machine.

The LEROS disc drives are independently driven and not mechanically linked by gears. This has two advantages; firstly, top and bottom disc geometries are identical, irrespective of creepage and secondly, disc speeds can be trimmed at weighing intervals during a test, thus enabling rates of creepage and contact stress to be maintained should disc diameters erode at different rates. The machine was also designed to exert high contact stresses, typical of the most severe wheel-rail contact, on wide *cylindrical* disc contacts. The resultant high contact stress results were of great interest.

The machine is based upon a standard Colchester Mascot 1600 lathe bed, using the gearbox driven lathe spindle for one disc drive. The original intention was that the wear machine components could be easily removed from the lathe bed thus freeing the lathe for other types of experimentation, however LEROS has been continuously used by numerous wear and fatigue researchers since its construction.

Under certain conditions, as experienced with testing on the Amsler machine (Chapter 6), LEROS discs developed periodic plastic deformations on wear surfaces. With reference to the types of Amsler disc deformations described in Chapter 6, similar patterns of facets and ripples were more clearly formed, but fine wavelength

corrugations did not form. The nature of these deformations and the test conditions which generated them, are discussed in Section 7.4, in conjunction with a vibration analysis of this machine.

7.2 A description of the LEROS machine.

A general view of the machine, set up for wear testing, is shown in Figure 7.1. Schematic views of LEROS, with the gearing arrangements for fast and slow speed tests, are shown in Figures 7.2 and 7.3, respectively. The respective frequencies of gear impacts are also listed. LEROS test discs were standardised to a size of 47mm diameter with 10mm wide wear tracks (Figure 7.4). 47mm is the maximum diameter a disc can be transversely machined from a (British Rail) rail head, with due allowance for clearance of any near-surface inhomogeneities. Similar discs were cut from transverse slices cut from rail wheel tyres (Figure 7.4).

Prior to testing, discs are separately bolted to the top and bottom disc drives on the respective bearing housings (Figure 7.5). After disc location, an environment chamber is fitted to the top disc bearing housing. The pivot assembly, containing the bottom disc bearing housing, can then be slid along the lathe bed until contact is made with an adjustable stop nut, at which point the disc wear tracks should be exactly aligned in the vertical plane (Figure 7.6). Unlike Amsler machine discs, this alignment adjustor means that any disc shoulder machining discrepancies can be compensated for and such discs are not wasted.

The bottom disc bearing housing is situated within a balanced pivot. A hydraulic ram pivots the bearing housing upwards and then exerts a force on the disc contact. The location of the ram and a schematic of the hydraulic system are shown in Figures 7.7 and 7.8. Once in position, the pivot housing is firmly fixed to the lathe bed by a central locking bolt and two bed end clamps (as is the top disc bearing housing). The pivot housing is moved along the lathe bed manually via a detatchable lever arm. The pivot housing contains an adjustable movement limit bolt. This ensures loaded contact ceases should either of the discs wear down to their shoulders. It is sturdy enough to take the full hydraulic load and has been used for experimentation on the

hydraulic system.

Disc drives.

The slower speed, top disc is driven, via the lathe spindle, from the lathe gearbox (powered by a 7.5kW AC motor). Two gear settings have been used for testing, giving top disc speeds of 403 rpm and 88 rpm. A bearing housing supports the disc drive head. This housing has been designed to minimise disc to bearing distance and to have the necessary rigidity for high contact stress tests. The disc is fitted to a slotted drive spigot. This in turn fits onto a slotted arbor which taper fits into the slotted drive head. This head is supported by roller bearings near the disc and by ball bearings away from the disc.

The rigid drive linkage between the lathe spindle and the drive head contains an EEL 2400 Series torque transducer that can measure up to 339Nm and is accurate to ±0.7Nm (Figure 7.3). Its millivolt output has been monitored on a W + W Chart Recorder. The torque calibration curve was determined by statically loading a beam that had been welded to a slotted disc and was thus accurately located on the top disc drive. This beam supported a weight stand, mounted on a knife edge pivot, 0.5m from the top disc axis. During calibration, the machine was slightly vibrated in order to increase the accuracy of the readings.

As with the Amsler modification, the torque transducer millivolt output is fed into a controllable Shape trip amplifier, this, in turn, is connected to the "emergency stop" circuit. If a set torque is exceeded on the lathe shaft, both the lathe and DC motors shut down and the hydraulic piston drops clear of the pivoting bottom disc bearing, thus allowing the discs to separate (i.e. power to the hydraulic powerpack is maintained). The spigot, arbor, drive head, both bearing sets and the torque transducer were all designed to be commercially available products for ease of replacement and minimum downtime.

The top disc drive linkage shaft is clamped in the lathe chuck in the normal fashion, but with a "drive" pin engaging one of the chuck clamps, so as to prevent any

slippage. The lathe gearbox and AC motor act as a "brake", rather than a "drive", as the bottom disc rotates at a faster speed. Braking force is from drive and gearbox friction and the "generator" resistance of driving the AC motor faster than normal. (In effect it is acting as a generator of electricity back into the grid.) This force overcomes the "sticking friction" at the disc interface and hence there is relative sliding between the discs.

The bottom "driving" disc bearing housing, drive components and bearings are identical to those in the top disc bearing housing. The bottom disc is driven, via gearing, by a thyristor controlled 4kW DC motor, supplied by Quinton Crane Electronics Ltd. (Figure 7.1). The motor control system contains a current limit safety device to prevent torque overload damage. The motor can be driven up to 2000 rpm. It is connected to the bottom disc drive assembly via one of two interchangeable Fenner gearboxes, inter-changeable pulleys and a toothed rubber belt (Figures 7.1, 7.2 and 7.3). A combination of the gearing ratios and pulley diameters results in motor:drive ratios of 4.287:1 (for 403 rpm tests with the lathe gearing set at "370 rpm") and 17.0:1 (for 88 rpm tests with the lathe gearing set at "87 rpm"). The gearing is such that up to 14% creepage can be generated between discs of equal diameter during a high speed test and up to 28% during a low speed test. One Fenner gearbox contains two cog wheels and the other three, therefore the rotational directions of the DC motor and its in-built tachometer have to be reversed when changing gearboxes. The DC motor is wired for this purpose, with a safety latched cross-over switch. The Fenner gearboxes are mounted on a keyed drive shaft which is, in turn, mounted in two bearings within the DC motor support frame. The shaft is connected to the sliding pivoting bottom disc bearing housing assembly by a variable length propulsion shaft with two universal couplings (Figures 7.5 and 7.6).

Both drive shafts are linked, via toothed belts, to Tekel TK510 shaft encoders. These register 360 square wave pulses per revolution. Their purpose was to facilitate computer control of the relative disc drive speeds, i.e. the DC motor would automatically follow variations in the lathe speed caused by fluctuations in mains voltage and disc contact friction. This facility was being developed during the

period of this work but was not available for the work described here; the DC motor speed was manually controlled. The encoders' outputs were used by an in-house tachometer, accurate to ±0.5 rpm. Its output was cross-checked by a Veeder-Root Type 6611 hand tachometer, which monitored the rotation of a small reflective patch on each disc drive and on the DC motor shaft. This had an accuracy of ±1rpm. Thyristor control of the DC motor speed control was via a (lockable) potentiometer, graduated in a 1000 divisions. Total shaft revolutions were counted by mechanical devices.

Hydraulic loading.

The loading system is shown schematically in Figure 7.8. The piston housing and manifold are in-house constructions. The piston annulus is a clearance fit so that, even at maximum pressure, there is a slight flow of oil around the piston, thus preventing any sticking. Pressurised flow to the piston is controlled by a Vickers electrically proportional pressure relief valve (which contains a linear displacement transducer) and a Vickers power amplifier board. One of two valves are used, dependent upon the load and degree of control required; one with a range from 2 to 63 bar and the other from 7 to 350 bar. The 2-63 bar system can exert loads up to 9 kN, giving a maximum contact stress of 1676 MPa between standard discs. The 7-350 bar system can exert loads up to 29 kN, giving a maximum contact stress of 3 GPa.

The system was removed from the wear machine and calibrated on a Mand tensile machine. For this work the system was manually controlled by a potentiometer. For the two valve pressure ranges, pressure transducers were fitted into the pressurised line to the piston. Their output is fed to a RDP controller/diplay unit. Although used as a pressure indicator, this can also function as a back-up control system if required. The calibration curves were slightly shifted as the oil temperature increased. By monitoring the RDP display, loads were manually trimmed during testing, so as to offset oil heating. (Subsequent to this work, the hydraulic power pack has been fitted with water cooling.)

During the initial LEROS test (Test 27), after re-fitting the loading system to the wear machine, it was noted that the pressure line to the piston housing was pulsing. The loading system was re-installed in the tensile machine and its pulse frequency was found to be around 50 Hz, with alarmingly high dynamic load amplitudes of up to ±1600 N (Figure 7.9). Numerous solutions were sought involving various forms of damping (eg. rubber) but to no avail. Eventually the radial piston pump within the power pack had to be discarded and replaced by a gear pump. This gave a fine pulse of 200 Hz with minimal dynamic amplitudes of ±6 N (Figure 7.9). However, the maximum load that could be applied was reduced from 38 kN to 29 kN. The gear pump produced more volume flow than the piston pump and a Sun controllable flow valve, which fed back the excess oil to the power pack, had to be fitted so that the system would function. The test was repeated (Test 28). Note that Tests 27 and 28 were carried out with the DC motor directly connected to the bottom disc drive. The test was repeated once more (Test 29) with a geared bottom disc drive, as described in previous section. The comparative results are given and discussed in Chapter 8.

Test environment.

As with Amsler Tests, all LEROS tests were carried out with a blast of dry compressed air on each wear track which cooled the discs and removed debris. The design of the environment chamber for LEROS is shown in Figure 7.10 and its location on the machine, clamped to the top bearing housing, can be seen in Figures 7.6 and 7.7. The perspex lid enabled observation of the discs during testing. The chamber is connected to a standard home vacuum cleaner, via a filter system. Its suction is such that a slight negative pressure exists in the chamber despite the air input, thus loose debris is drawn away from the wear interface. The filter system and environment monitoring system are as described in Section 6.2, except that the steady air pressure during testing was 3.1kg/cm^2 (44 psi) and the air was more extensively dried and filtered. Disc bulk temperatures were measured by a contact thermometer. Even under the severest test conditions, discs did not exceed 7°C above room temperature. Blockage of the vacuum flow by coarse debris collecting in the filter would affect the test; such a blockage was reflected by a change in the torque curve. In a few severe tests, the filter was cleared during testing, between the

measuring stages. (Since this work, the filter has been re-designed so as to allow air flow around any blockage.) Air leaving the environment chamber was monitored, with respect to temperature and humidity, using a Testoterm Hygrotest 6200. As with the Amsler tests (Section 7.4.1), the limited variations in humidity and temperature that occurred during each test did not seem significantly to affect the coefficient of traction. Figure 7.11 shows the relationship between traction coefficient and environment chamber conditions (relative humidity and temperature), for the same material combination over a range of test conditions.

7.3 The LEROS test programme.

The test programme is shown in Table 7.1. Top and bottom discs of the same disc geometry were used throughout. The top disc drive torque (used to calculate the coefficient of traction) and conditions in the environment chamber (humidity and temperature) were monitored during every test. The aim of the programme was as follows:

1. To compare of the wear behaviour of the three bainitic steels with standard rail steel with respect to variations in contact stress and creepage.
2. To compare the results of tests on the two wear machines under indentical conditions of contact stress and creepage (albeit on different disc geometries).
3. To assess the materials under conditions of high contact stress which are outside the range of the Amsler machine for its standard disc geometry. The creepage value of these tests was kept low, such that the product of maximum contact stress and creepage ($p_o\gamma$) was the same as in earlier tests. Other workers[Bolton et al, 1982; Bolton and Clayton, 1984] have used this product in the evaluation of dry, air-cooled, rolling-sliding wear test results.
4. To assess the materials with a combination of high contact stress and creepage that is again outside the range of the Amsler machine for standard disc geometries.
5. To assess the effect of changing the test speed (from 403 to 88 top disc rpm). One pair of such tests was carried out under the high creepage, low contact stress conditions which had generated the maximum degree of regular surface plastic deformations in Amsler discs. These results were used as part of the vibration

analysis of the machine.

6. To assess the effect of reversing top "driven" and bottom "driving" disc materials for a standard set of conditions.

7. Although not originally intended as part of the test programme (as discussed in Section 7.2), the initial test was repeated with a change in the hydraulic load supply system (i.e. a change in the dynamic loading of the disc contact). It was then repeated once more with a change in the bottom disc drive system. These results were compared. The loading and drive systems of this last test were used throughout the rest of the test programme.

7.4 A vibration analysis of LEROS.

This analysis was based upon experience gained from vibration analyses of the Amsler wear machine, as described in Appendix I[Garnham, Brightling and Beynon, 1988] and in Section 6.5. The machine was examined as follows:

* Statically with external excitation.
* With just the hydraulics running.
* With just the lathe motor idling.
* With the hydraulics running and both drives free running, i.e. no disc contact.
* Under test conditions.

Assessments were carried out at the two machine speeds used in the wear test programme; top disc rotations at 403 rpm (6.72 Hz) and 88.2 rpm (1.47 Hz). The test conditions used were those which resulted in the clearest disc surface plastic deformations during the Amsler wear test programme and initial vibration analysis.

Experimental procedure

Vibration measurement.

A single accelerometer was used, fitted with a magnetic base (Bruel and Kjaer Type A4328 {No. 92062}). It was coupled to a pick-up preamplifier (Bruel and Kjaer Type 2625, set at 28V) and this in turn was coupled to a Fast Fourier Transform Frequency Analyser (Ono-Sokki CF-910). The preamplifier could be set to output acccelerations, velocities (the first integral of accelerations with respect to time) and

displacements (the double integral of accelerations with respect to time). This integration process can be viewed as a progressive low-pass filter of the frequency spectrum, reducing amplitudes at higher frequencies. In this analysis, acceleration and some velocity spectra have been assessed. Displacement spectra amplitudes (mV outputs) were too low to measure.

For static and dynamic tests, the accelerometer was alternately located adjacent to the large bolts which secure each bearing housing to the lathe bed (Figures 7.12a & b). These are the only flat locations on each bearing housing. Vibrations solely due to hydraulic loading, with the rest of the machine switched off, were measured adjacent to the top safety bolt (Figure 7.12c). This had been screwed down, so that it was loaded hydraulically via the bottom bearing housing. For most dynamic measurements, 256 spectra were measured and averaged by the frequency analyser, but for some it was 64 spectra. For static tests, where the machine was externally excited, an average of 64 spectra was taken; each reading being automatically triggered by the external soft hammer blow. In this instance, the mV output relating to signal power was dependent upon the arbitary power of each blow, therefore it is the pattern of relative amplitudes which is significant.

LEROS disc periodic plastic undulations ... a brief review.

Full results are shown in Table 7.2 and undulation patterns are mapped against test conditions and materials in Table 7.3. Except where indicated, these results refer to the disc shape at the end of the test. Some discs developed facets and ripples during a test, which were then either subsequently cleared or modified. Amsler type corrugations (shallow undulations extending across the complete track width, with wavelengths in the order of 0.3mm) were *not* seen during any LEROS tests. Comparative Amsler results are shown in Tables 6.3 and 6.4.

Undulation wavelengths

The fact that facet wavelengths were similar for all the materials at *both* machine speeds was of great interest. Ripples, which dynamically formed and cleared during severe creepage tests, *also* had similar wavelengths. These results are represented on

the "test condition maps" shown in Table 7.3. The clearest facet and ripple conditions *during* a test were used to construct these maps.

Undulation frequencies

These constant wavelengths gave, at the higher LEROS speed of around 403 rpm, facet frequencies of between 180 and 260 Hz, and at the lower LEROS speed of around 88 rpm, facet and ripple frequencies of between 40 and 65 Hz.

Undulation patterns

Some discs generated a regular pattern of facets around the circumference (eg. Figure 7.13) and, once generated, the basic pattern generally remained throughout the test. The circumferential position of the facet peaks remained stationary for the complete length of some tests and for periods of others. This was determined by observing the positions of certain marked peaks during a test, with respect to the disc drive keyways and by stroboscopic light examination during testing.

During some tests, after a period where the circumferential pattern of facet peaks was constant, some alternately spaced peaks slowly migrated circumferentially to form patterns of double and/or triple peaks. A mid-test disc with regular peaks is shown in Figure 7.14 and the same disc at the test end, after some peak migration, is shown in Figure 7.15.

Some discs developed a degree of eccentricity with respect to facet amplitudes and a few developed an eccentric, complex, double pattern of undulations (Figure 7.16).

Undulation characteristics

The surface features of dark, oxidised facet peaks, and of facet troughs with a mixed abraded, oxidised and metallic appearance, were common to all faceted discs (Figures 7.13 and 7.14). Surface flaking was often prominent from the trailing edge (with respect to sliding) of facet peaks. Microexamination of faceted discs, of different materials, showed that there was a higher degree of matrix strain beneath facet peaks.

At one test condition (1300 MPa maximum contact stress, 10% creepage) distinct ripples formed on top driven discs, irrespective of material. Ripple formation is typical of the "severe wear" mechanism described by Bolton and Clayton[1984]. The ripple patterns had no common surface characteristics, as can be seen from Figures 7.17a, b and c and Figure 7.18b. The most wear resistant disc, B52, changed wear characteristics when tested under these severe conditions, from being initially faceted (7.18a) to finally rippled (Figure 7.18b), thus suggesting a transition from one wear regime to another. Disc rippling had a certain degree of periodicy which was close to that of faceting (Tables 7.2 and 7.3).

The test discs assessed in the vibration analysis.

Test conditions of 500 MPa maximum contact stress and 10%creepage were chosen, as these generated clear surface plastic deformations during the Amsler vibration analysis tests. From Table 7.2 it can be seen that severe undulations were generated in the top disc during the high speed test, but only shallow top disc undulations during the slow speed test (which were barely visible on the disc surface). There was considerable facet peak migration during the high speed test (Figure 7.19) plus growing disc eccentricity.

A brief review of the vibration spectra results.

The dominant frequencies for each set of test conditions are given in Tables 7.4 to 7.8. Acceleration spectra were examined over different frequency ranges for each set of vibration test conditions; velocity spectra were examined for most test conditions. Displacement amplification was too low for analysis.

Natural machine resonances - Table 74.

The machine was switched off. It was excited by blows from a "soft" hammer on to the lathe bed between the bearing housings. The strongest acceleration and velocity signals, measured on both bearing housings, were at 85 and 150 Hz, however there were other strong signals over a wide range of frequencies (Figure 7.20).

Resonances from individual rotating machine componenets.

Principal resonances are summarised in Table 7.5. LEROS components are described schematically in Figures 7.2 and 7.3 for the two speeds used, along with a breakdown of respective gear-trains and resultant gear-tooth impact frequencies. The top and bottom needle roller bearings nearest the discs, contain 28 rollers each. If static, this would result in contact frequencies of 41 and 188 Hz, respectively, at the slow and fast speeds. However, the movement of rollers within the bearing cages results in lower contact frequencies.

The major acceleration frequency (around 5700 Hz) measured, on either bearing housing, originated from the lathe AC motor (including the pulleys and gears up to the clutch). Until facets developed, it was also the strongest signal during the vibration assessed wear tests. The strongest velocity signal (of around 43 Hz) was also generated by the AC motor. (This lies just within the faceting frequency range, 40 to 65 Hz, for low speed tests; this is reviewed later.) The spectra are shown in Figure 7.21. This pattern was not affected significantly by engaging either of the two lathe drive gear-trains.

The hydraulic system, loaded at the test setting, generated only a small amount of "noise", with acceleration spectra at multiples of 100 Hz (Figure 7.22). Engaging the DC motor drive at the slow speed setting reinforced the 300 Hz acceleration signal (nearest tooth impact frequency, 153 Hz - Figure 7.3) and the 27-30 and 300 Hz velocity signals. Engaging the DC motor at high speed setting reinforced the 200 and 300 Hz acceleration signals and the 30, 155, 200 and 300 Hz velocity signals (Figure 7.23). There were no matching gear tooth impact frequencies in the high speed Fenner gearing. **Note** that these signals are at a fraction of the strength of those generated by the idling lathe AC motor.

Resonances from the machine running, as set for testing, but with no loaded disc contact.

The results for the high test speed setting are summarised in Table 7.6. The dominant acceleration and velocity signals, from both bearing housings, were those

of the lathe AC motor (described above). An additional significant signal of 285 Hz, for both acceleration and velocity, was measured on the bottom bearing housing. There were no gear tooth impacts around this frequency. (This frequency lies a little above the range of faceting frequencies found in high speed tests, 180 to 260 Hz; this is reviewed later.)

The results for the low speed setting are also shown in Table 7.6. As above, acceleration (5500 to 6200 Hz) and velocity (43 Hz) signals emanating from the lathe AC motor were dominant and at the same strength as at high speed. There were *no* signals around 285 Hz at this low speed.

Resonances from a loaded high speed test.

Disc facet data and vibration results during the test are given in Table 7.7. Some acceleration and velocity spectra at the test end are shown in Figures 7.24 and 7.25, for the top and bottom bearing housings, respectively. The strongest accelerations measured on the top bearing housing originated from the AC motor. These increased in strength during the test (as disc facets developed). Velocities were only measured at the end of the test. At this point, although the "AC motor" velocity of 43 Hz was significant, there were stronger signals in the ranges 125 to 150 Hz and 215 to 225 Hz. Strong accelerations also developed at these frequencies after being of negligible strength at the start of the test. These match the frequencies of top disc facets which developed during the test (Table 7.7). A strong acceleration and velocity signal, at 1375 Hz on the top bearing housing, also grew during the test. This might be the 6th harmonic of 225 Hz.

Strong accelerations of the bottom bearing housing were spread over a wide range of frequencies between 95 and 6000 Hz (Figure 7.25, Table 7.7). The strongest test end velocities were at the faceting frequencies, except for some strong low frequency signals between 6 and 14 Hz; this might reflect bottom disc eccentricity. (At the test end, the bottom disc was revolving at 441.3 rpm, i.e. 7.36 Hz.)

It appears that the strength of velocity signals most accurately reflects the

development of severe disc surface deformations. These signals were not present when the machine was run without discs, or at the start of this loaded test, however frequencies at, or near, these ranges have featured in the unloaded machine assessment described above.

To recap:

* The machine has a natural resonance around 150 Hz.
* 200 and 300 Hz acceleration and velocity signals and a 155 Hz velocity signal were amplified by the combination of weak hydraulic load vibrations and the DC motor gear-train operating at high speed.
* 285 Hz acceleration and velocity signals were measured on the bottom bearing housing when the machine was run without discs at high speed.

However, the fact that facet wavelengths are not affected by machine speeds casts doubt on whether any of these factors are significant with respect to facet formation; they may enhance facet amplitudes at the high speed setting.

Resonances from a loaded low speed test.

Disc facet data and vibration results during the test are given in Table 7.8. Top and bottom bearing housing frequency spectra, for the unloaded machine and the loaded machine (mid-test), can be compared in Figures 7.26* and 7.27, respectively. (* The spurious signal at 8100 Hz, caused by a rubbing metallic seal, should be ignored.)

Only slight top disc facets developed during this test. The low facet amplitudes remained constant from mid-test to the test end. There was only a faint visual indication of this faceting. No bottom disc facets developed. From the Tables 7.6 and 7.8, and from Figure 7.26, it can be seen that the spectral patterns from the bearing housings of the unloaded machine remained during the loaded test. There was a minor velocity signal from both bearing housings, near the faceting frequency of 60 - 70 Hz, observed at the same low signal strength, both at mid-test and at the test end. However, this signal was present when the machine was run without discs. There were no acceleration signals at the faceting frequecies.

This test gave no indication as to why the disc faceted. Most low speed facet frequencies were near, or at, the strongest velocity signal (emanating from the AC motor) of 43 Hz (Figure 7.2).

Summary of vibration results.

* On LEROS, facet wavelengths (≈4.5mm) remained constant at both test speeds, i.e. facet frequencies changed proportionally. On the Amsler wear machine (for a limited comparative test), facet frequencies remained constant at both test speeds, and facet wavelengths (≈12mm at high speed and ≈6mm at low speed) changed proportionally, however the wavelengths of the Amsler disc fine corrugations (see Chapter 6 and Appendix I[Garnham et al, 1988]) remained constant (≈0.3mm) at both speeds, with a proportional change in high corrugation frequencies.

* Where test parameters were the same, facet amplitudes were far lower at the respective lower test speeds set on both machines. LEROS facet frequencies were within the range of 180 to 260 Hz at a top disc speed around 6.72 Hz and within the range of 40 to 65 Hz at a top disc speed of around 1.47 Hz. This applied over the full range of test conditions and material combinations (Table 7.2). Amsler faceting behaviour was more variable (see Chapter 6 and Appended I).

* Mass, semi-periodic, plastic flow of disc wear surfaces on LEROS, described as "rippling" and typical of a "severe wear regime"[Bolton and Clayton, 1984], resulted in surface undulations with the same order of wavelength as the respective disc facets. Under these severe test parameters, the machine was only run at the slower speed.

* Limited maps of facet formation (Table 7.3), with respect to disc materials and test parameters of maximum contact stress and creepage, give a slight indication that the range of test conditions required for facet formation might be related to bulk material properties such as hardness (Tables 2.3). Microsections through faceted discs are described in Chapter 9 and the mechanism for their formation is discussed in Chapter 10.

* The strongest vibration frequencies, for both accelerations and velocities, emanating from LEROS, were generated solely by the lathe AC motor and associate gearing up to the clutch mechanism. These were the acceleration frequencies within the range of 5000 to 6500 Hz and the velocity frequencies close to 43 Hz.

* When facets are generated on either wear machine, the strength of velocity frequency signals gives the clearest indication of their presence and growth. Acceleration frequency spectra register the presence of facets, but there can be stronger machine signals, particularly on LEROS.

* It has *not* been established that machine resonances, natural or generated, are responsible for facet formation. LEROS has natural resonances at frequencies bordering the high speed faceting frequency range, in addition to limited excitation near the top end of the range (from the bottom disc drive, via the DC motor and Fenner gearing, under hydraulic loading). The strongest velocity frequencies generated by LEROS (at both speeds), of around 43 Hz, lie at the lower end of the faceting / rippling frequency range, for the slower machine speed.

* The distribution of rollers in the bearings closest to the discs nearly matches the circumferential distribution of facets around the discs. However, the rollers are not static within the bearing housings, therefore loaded contact frequencies would be lower than facet frequencies.

8.5 Lubricated test facet patterns.

Subsequent to the work described in this thesis, the author has carried out water-lubricated, rolling-sliding contact fatigue tests on the LEROS wear machine, using the same design of disc[Garnham and Beynon, 1990 - Appendix II; Beynon et al, 1994]. Under many test conditions, a visually apparent "facet pattern" developed on the wear track of the more fully oxidised bottom "driving" discs. The amplitudes of such undulations were barely measurable and most were less that 2μm. The wavelengths of these facet markings were either similar to those found in the dry tests, or double. All these tests were carried out at the higher machine speed. Microscopic examination of the

oxidised disc surfaces indicated that there had been a "stick-slip" pattern of disc contact and wear (Figure 7.40).

7.6 Summary comment on LEROS

A twin disc, rolling-sliding wear machine has been succesfully built on to the bed of a standard lathe. Its robust design and construction, together with independent disc drives, enables tests to carried out with minimal variations to the distribution of contact stress and creepage. For the tests described in the present work, the electronic disc drives were manually controlled via potentiometers and during some tests there was a little creepage variation. Subsequent to the present work, automatic control was successfully fitted[Garnham and Beynon, 1990 - Appendix II].

As seen on the modified Amsler machine, under certain conditions, clear undulations (facets) form on LEROS disc surfaces. No direct vibration frequecy linkage to the disc drive gear trains has been established.

7.7 References.

Beynon, J.H., Garnham, J.E. and Sawley, K.S. (1994). "Rolling contact fatigue of four pearlitic rail steels." To be published. Initially submitted to *WEAR*, August 1994. Re-submitted following review, June 1995.

Bolton, P.J., Clayton, P. and McEwen, I.J. (1980). "Wear of rail and tyre steels under rolling-sliding conditions." *Proc. ASME/ASLE Lubrication Conf., San Francisco, USA, 18-21/08/80.* Pub. *ASLE Trans.* 25 (1), pp. 17-24.

Bolton, P.J. and Clayton, P. (1984). "Rolling-sliding wear damage in rail and tyre steels." *WEAR* 93, pp. 145-165.

Garnham, J.E., Brightling, J.R. and Beynon, J.H. (1988). "Rolling-sliding dry wear testing - a vibration analysis." *WEAR* 124, pp. 45-63 (appended - Appendix I).

Garnham, J.E. and Beynon, J.H. (1990). "The early detection of rolling-sliding contact fatigue cracks." *Proc. 3rd. Int. Symp. on "Contact mechanics and wear in rail-wheel systems", 22-26/7/90, Univ. of Cambridge (UK).* Pub. *WEAR* 144 (1991), pp. 103-116 (appended - Appendix II).

Tyfour, W.R., Beynon, J.H. and Kapoor, A. (1995a). "The steady state wear behaviour of pearlitic rail steel under dry rolling-sliding contact conditions." *WEAR* 180, pp. 79-89.

Test No.	Top driven disc	*Initial values* Max. cont. stress p_o (Mpa)	Creep -age. γ (%)	$p_o\gamma$	Test length (x1000 bottom disc revs.) + speed.		COMMENT
							Mild wear regime tests.
27	R52	500	3	15	160	fast	" Oscillating hydraulic load. Direct DC motor drive to bottom disc.
28	R52	500	3	15	160	fast	" Steady hydraulic load. Direct DC motor drive to bottom disc.
29	R52	500	3	15	160	fast	" *Steady* hydraulic drive. *Geared* DC motor drive to bottom disc. *These conditions prevailed for all other tests given below.*
33	B04	500	3	15	160	fast	"
34	B20	500	3	15	160	fast	"
35	B52	500	3	15	160	fast	"
30	R52	900	3	27	100	fast	Transitional wear regime tests.
31 *	W64 on R52	900	3	27	100	fast	" (Disc materials reversed.)
30B	R52	900	3	27	50	slow	" (Repeat test at slow speed.)
36	B04	900	3	27	100	fast	"
37	B20	900	3	27	100	fast	"
38	B52	900	3	27	100	fast	"
46	R52	1800	1.5	27	40	slow	Same $p_o\gamma$ with high p_o.
47	B04	1800	1.5	27	40	slow	"
48	B20	1800	1.5	27	40	slow	"
49	B52	1800	1.5	27	40	slow	"
32	R52	1300	3	39	40	slow	Higher p_o transitional wear tests.
39	B04	1300	3	39	40	slow	"
40	B20	1300	3	39	40	slow	"
41	B52	1300	3	39	40	slow	"
51	R52	500	10	50	100	fast	LEROS vibration analysis tests.
52	R52	500	10	50	100	slow	"
30A	R52	900	7	63	50	slow	Transitional test, higher creepage.
42	R52	1300	10	130	12.5	slow	Severe wear test.
43	B04	1300	10	130	7.5	slow	"
44	B20	1300	10	130	10	slow	"
45	B52	1300	10	130	10	slow	"

* Bottom driving discs were W64 except for Test 31.

Table 7.1 LEROS wear test programme.

Table 7.2 LEROS test disc deformations, including periodic undulations, generated during the test programme. Test conditions are shown.

Test Number		[a] 28	33	34	35	30	30B	36	37	38	46	47
Top braking disc		R52	B04	B20	B52	R52	R52	B04	B20	B52	R52	B04
Bottom driving disc		W64	W64	W64	W64	W64	W64	W64	W64	W64	W64	W64
Initial max. contact stress, p_o, (MPa)		500	500	500	500	900	900	900	900	900	1800	1800
Initial creepage, γ, (%)		3	3	3	3	3	3	3	3	3	1.5	1.5
Nominal $p_{o\gamma}$ (MPa)		15	15	15	15	27	27	27	27	27	27	27
Test speed (top disc Hz)		6.72	6.72	6.72	6.72	6.72 6.72	1.47	6.72 6.72	6.72 6.72	6.72 6.72	1.47	1.47
Profiled at (bottom disc cycles X 10^3) (ie, at the test end unless indicated~)		160	160	160	160	50~ 100	50	50~ 100	50~ 100	50~ 100	40	40
Track width spread (%)	Top	0.8	1.4	0.6	0.2	- 6.4	4.3	- 5.9	- 3.6	- 1.5	20.8	12.3
	Bottom	1.9	1.5	1.3	0.6	- 6.9	3.7	- 6.6	- 15.7	- 7.1	23.0	20.0
Disc eccentricity (µm) [b]	Top	2	15	2	1	24 50	18	38 50	42 90	3 43	17	5
	Bottom	5	4	7	4	5 16	14	15 30	26 37	9 20	180e	153e
Max. amplitude of long wave-length undulations (±µm) [c]	Top	3F	13F	-	-	30F 65F	26F	3.5F 4.5F	50F 80F	- 76F	-	-
	Bottom	2.5i	-	-	-	7F 14F	-	48F 86F	6.5F -	- 16F	-	-
Facets (or Ripples) per circumference [d]	Top	37p	34	-	-	33 31	33	37p 15p	38 38	- 36p	-	-
	Bottom	-	-	-	-	34p 35	-	36 36	15p -	- 30p	-	-
Facet "double peaks" [e]	Top	-	-	-	-	- 11	-	- -	- 9	- 4p	-	-
	Bottom	-	-	-	-	- -	-	1 14	- -	- 16p	-	-
Facet (or Ripple) frequency	Top	249	228	-	-	222 208	48.5	108 101	255 255	- 242	-	-
	Bottom	-	-	-	-	235 242	-	252 249	104 -	- 202	-	-
Max. amplitude of short wave-length undulations (±µm) [f]	Top	0.5	nm	<0.5	0.5	nm nm	nm	1 1	nm nm	<0.5 nm	70	1
	Bottom	4	2	3.5	2.5	nm nm	4.5	nm nm	3 7	4 14	23	20

Test Number		48	49	32	39	40	41	51	52	30A	42	43	44	45
Top braking disc		B20	B52	R52	B04	B20	B52	R52	R52	R52	R52	B04	B20	B52
Bottom driving disc		W64	W64	W64	W64	W64	W64	W64	W64	W64	W64	W64	W64	W64
Initial max. contact stress, p_o, (MPa)		1800	1800	1300	1300	1300	1300	500	500	900	1300	1300	1300	1300
Initial creepage, γ, (%)		1.5	1.5	3	3	3	3	10	10	7	10	10	10	10
Nominal $p_{o\gamma}$ (MPa)		27	27	39	39	39	39	50	50	63	130	130	130	130
Test speed (top disc Hz)		1.47	1.47	1.47	1.47	1.47	1.47	6.72 6.72	1.47 1.47	1.47	1.47	1.47	1.47	1.47
Profiled at (bottom disc cycles X 10^3) (ie, at the test end unless indicated~)		40	40	40	40	40	40	60~ 100	60~ 100	50	12.5	7.5	10	10
Track width spread (%)	Top	7.5	8.3	10.9	8.3	5.8	3.6	- 6.1	- 3.7	5.4	22.6	14.9	10.5	5.5
	Bottom	28.7	31.7	10.0	12.7	10.1	16.9	- 4.4	- 2.4	4.3	18.6	31.3	47.2	34.8
Disc eccentricity (µm) [b]	Top	13	21	45	70	37	68	28 150	16 18	23	46	22	2	26
	Bottom	170e	270e	42	52	48	75	24 31	10 11	20	32	90	106	80
Max. amplitude of long wave-length undulations (±µm) [c]	Top	-	-	14i	15F	40F	71F	170F 190F	4.5F 4.5F	16F	13.5Ri	70R	53R	40R
	Bottom	-	-	-	-	-	-	2.5F 4.5F	- -	-	-	76R	58i	-
Facets (or Ripples) per circumference [d]	Top	-	-	-	31p	36	38p	27 26	48p 42p	43	-	29	36	38
	Bottom	-	-	-	-	-	-	12p 12p	- -	-	-	26	-	-
Facet "double peaks" [e]	Top	-	-	-	-	1	8p	7 8	- -	-	-	-	-	-
	Bottom	-	-	-	-	-	-	- -	- -	-	-	-	-	-
Facet (or Ripple) frequency	Top	-	-	-	45.6	52.9	55.9	181 175	70.6 61.8	63.2	-	42.6	52.9	55.9
	Bottom	-	-	-	-	-	-	89 89	- -	-	-	42.2	-	-
Max. amplitude of short wave-length undulations (±µm) [f]	Top	34	26	nm	nm	nm	nm	nm nm	1 2	nm	3	nm	nm	nm
	Bottom	15	35	8	8.5	12	21	1 6	2 2.5	3	5	nm	nm	49

[a] : The Test 29 discs were damaged and not profiled. The results for a similar test are given. Test 28. The tests differed in that the Test 28 bottom disc had a direct drive, not a geared drive.

[b] : "e" - reading larger than profilometer scale; an estimate has been given based upon profile extrapolation and micrometer measurements.

[c] : "F" - long wavelength, track-wide corrugations formed, termed "facets".
"R" - long wavelength, regular ripples formed ("sand-dune" effect).
"i" - irregular undulation wavelengths.

[d] : Although initially regularly spaced, some facet peaks migrated during testing and "double peaks" formed.

[e] : "p" - only part of the circumference has a clear pattern of regular undulations; the data given has been extrapolated to represent the full circumference.

[f] : On the LEROS machine this represents maximum surface roughness; no short wavelength corrugations formed on any LEROS discs. On some discs, where steep undulations had formed, surface roughness could not be measured ("nm").

Maximum contact stress (MPa)	Creepage 1.5%	3%	7%	10%
R52 / W64				
500		(F4.0/none)		high wear (F5.4/none)^{fast} mild wear (F3.0/none)^{slow}
900		(F4.5/4.3)^{fast} [(F4.7/4.1)]^{a} (F4.5/none)^{slow}	(F3.3/nil)^{slow}	
1300		(none/none)^{slow}		(R4.5/R5.0)* (* ripples sheared during test)
1800	(none/none)^{slow}			
B04 / W64				
500		(F4.3/none)^{fast}		
900		(F4.0*/4.1)^{fast} (* top disc faceting for initial 40000 revs only)		
1300		(F4.7/none)^{slow}		(R4.9/R5.4)^{slow}
1800	(none/none)^{slow}			
B20 / W64				
500		(none/none)^{fast}		
900		(F3.8/none)^{fast}		
1300		(F4.0/none)^{slow}		(R4.0/none)^{slow}
(R4.0/nil)^{slow}				
1800	(none/none)^{slow}			
B52 / W64				
500		(none/none)^{fast}		
900		(*F4.1/4.9)^{fast} (* faceting for last 50000 revs only)		
1300		(F3.9/none)^{slow}		(R3.9/none)^{slow}
1800	(none/none)^{slow}			

KEY:

(F4.0/none)	: (top disc facets, average wavelength 4.0mm / bottom disc, no facets formed)
fast	: fast machine speed, 403rpm, 6.72 Hz
slow	: slow machine speed, 88.2 rpm, 1.47 Hz.
(R4.0/R4.1)	: (top disc ripples, average wavelength 4.0mm / bottom disc ripples, av. wavelength 4.1mm)
a	: In this test the materials were reversed, W64 top disc and R52 bottom disc.

Table 7.3 Test condition map for LEROS disc undulations.

MACHINE NATURAL RESONANCE - STATIC DISC CONTACT AND NO CONTACT

A 801 N load was applied to two 47 mm diameter cylindrical discs with 10 mm wide wear tracks in contact, resulting in a maximum contact stress of 500 MPa. 4 Nm of torque was applied to the top disc shaft in the direction of (dynamic) testing. (This was the maximum torque applicable at this load before inter-disc slippage occurred.) The machine was excited by repeated upward soft-hammer blows to the Lathe bed between the bearing housings. With manually applied hammer blows the value of signal amplitudes is arbitary, however a valid averaged pattern of amplitudes over the frequency spectrum is established, as shown by the mV readings given below. For each spectrum an average of 64 hammers blows was taken.

Transducer Location	Principal Frequencies (Hz)	Signal Strength (mV)
Top bearing housing		
Accelerations:	85	1.7
	150	1.7
	220, 340, 430, 695, 835, 885, 1000, 1155, 1360	0.8 → 1.0
	25, 2400-2700, 3500-3700, 5500-6500	≃ 0.3
Velocities:	85	0.62
	150	0.52
	25	0.48
	55	0.24
	220-225	0.10
Bottom bearing housing		
Accelerations:	150	2.2
	350-365	1.8
	85	1.7
	25, 55, 435, 850, 1000	0.6 → 1.0
	5000-5200	≃ 0.3
Velocities:	150	0.80
	85	0.67
	25	0.54
	55	0.40
	365	0.30
	190-225	0.25

Frequency spectra for the natural machine accelerations with NO discs present were not significantly different from those above except that signals around 85 Hz were of low amplitude. Velocity spectra were not measured.

Table 7.4 Principal frequencies of natural resonances from LEROS, measured as accelerations and velocities, with the machine components static.

MACHINE COMPONENT RESONANCES

Lathe AC motor idling, clutch disengaged - gear shafts static

Transducer location	Principal frequencies (Hz)	Signal strength (mV)
Top bearing housing		
Accelerations:	5725	22
	5500-6200	>11
	45, 100	2.6
Velocities:	43	1.9
	100	0.9

This pattern was not affected by any of the gearing selections.

Lathe drive engaged at 400 rpm

Top bearing housing		
Accelerations:	5200	26
	5725	13
	4900-5900	> 8
	475, 575, 900, 1375, 2300, 2700	6 → 9
	45, 100	4

Velocities not measured.

Lathe shaft engaged at 88 rpm

Top bearing housing		
Accelerations:	5275	21
	5725	18
	5100 → 6000	> 10
	2375	8
	50	5
	600, 975, 1350, 1775	≃ 3

Velocities not measured.

Hydraulic loading only (801 N)

Bottom bearing housing		
Accelerations:	400	0.14
	200, 700, 900, 1200	0.06 → 0.08
	50, 100, 140, 300, 500, 600, 800, 1000, 1100	0.02 → 0.05

Velocities not measured.

Bottom shaft rotating at 97.5 rpm (DC motor 1658 rpm), hydraulically loaded against stop at 801 N.

Bottom bearing housing		
Accelerations:	300	1.9
	870	1.2
	30	0.9
	200	0.8
	1170	0.6
Velocities:	27.5	0.84
	300	0.31

Bottom shaft rotating at 883.2 rpm (DC motor 1900 rpm), hydraulically loaded against stop at 801 N.

Bottom bearing housing		
Accelerations:	300	2.6
	200	2.0
	825, 1000	≃1.8
	155	1.3
	30	0.5
Velocities:	155	0.56
	200	0.48
	300	0.42
	30	0.38

Table 7.5 Principal frequencies of resonances generated by the individual operating components of LEROS, measured as accelerations and velocities.

MACHINE RUNNING EMPTY UNDER TEST CONDITIONS

(Hydraulic ram loaded against the bottom bearing housing stop bolt.)

High speed conditions (as in Test 51)

801 N load
Top disc shaft 401.2 rpm (6.69 Hz). Spindle tooth impacts 455 Hz.
Bot. disc shaft 443 rpm (7.38 Hz). Final gear tooth impacts 827 Hz.

Transducer location	Principal frequencies (Hz)	Signal strength (mV)
Top bearing housing		
Accelerations:	5550	28.3
	5000 → 6000	> 12.0
	475, 575	7.5
	900, 1340, 2325	≃ 6.0
	45, 285	3.5
	100, 150, 200, 300, 670, 970, 1190	1.7 → 2.7
Velocities:	42.5	2.3
	17.5, 32.5, 92.5, 150, 200, 285, 475, 570	0.4 → 0.7
Bottom bearing housing		
Accelerations:	5550	9.4
	5100 → 6000	> 5.0
	285	6.2
	570	4.1
	150	2.9
	45, 100, 200, 350, 825, 855, 1000, 1135	1.5 → 2.4
Velocities:	42.5	1.5
	285	1.0
	147.5	0.8
	17.5, 100	0.6
	200, 300, 567.5	≃ 0.4

Low speed conditions (as in Test 52)

801 N load
Top disc shaft 88.4 rpm (1.473 Hz). Spindle tooth impacts 131 Hz.
Bottom disc shaft 97.7 rpm (1.628 Hz). Final gear tooth impacts 164 Hz.

Transducer location	Principal frequencies (Hz)	Signal strength (mV)
Top bearing housing		
Accelerations:	5725	25.9
	5500 → 6200	> 13.0
	2375, 7050	7.4
	45, 670, 1190, 1785	2.2 → 2.7
	100, 200, 300, 595	1.4 → 1.7
Velocities:	43	2.1
	27.5, 100	≃ 0.9
Bottom bearing housing		
Accelerations:	5600	10.1
	5300 → 6500	> 5.0
	45	2.2
	110, 300, 1190	≃ 1.9
	415, 595, 885	1.4 → 1.6
Velocities:	43	1.5
	18.5, 27.5, 111.5	0.6 → 0.7
	100.5, 130	≃ 0.3

Table 7.6 Principal frequencies of the resonances generated by LEROS with the machine running under load against the safety stop with no discs fitted. Measured as accelerations and velocities; top - at the higher speed, bottom - at the lower speed.

VIBRATION MONITORING OF A HIGH SPEED TEST

Test 51: BS11 rail steel top disc. Type 'D' tyre bottom disc. maximum contact stress 500 MPa. creepage 10%. test length 10^5 top disc revolutions.

	Load (N)	Top disc speed (rpm)	(Hz)	Bottom disc speed (rpm)	(Hz)
Test start:	800	401.5	6.69	443.8	7.40
Test end :	786	401.2	6.69	441.3	7.35

At each weighing interval, the load and DC motor speeds were trimmed so as to maintain contact stress and creepage with respect to the different worn diameters of the discs and slight variations in Lathe speed.

Frequencies and maximum amplitudes of facets that formed on the worn disc surfaces:

	Top disc		*Bottom disc
Frequencies at 60,000 revs.	Half circumference ≃ 139 Hz		89 Hz
	Half circumference	214 Hz	smooth
Max. amplitude :	± 170 μm		± 2.5 μm
Frequencies at 100,000 revs.	Half circumference	167 Hz	89 Hz
	Half circumference	181 Hz	smooth
Max. amplitude :	± 190 μm		± 4.5 μm

* Note: Bottom disc facet amplitudes were two orders of magnitude smaller than top disc facet amplitudes.

Transducer location	Principal Frequencies (Hz)	Signal strength (mV) (Top disc revs X1000) ≃3	≃65	≃105
Top bearing housing				
Accelerations: (10 kHz range)	5550	27	43	61
	5300 → 5800	>12	>25	>30
	1375	7	53	65
	1250 → 1475	<5	>30	>35
	215-225	7	64	41
	125-150	<6	20	32
	95	<6	7	9
	45	<6	4	5
Velocities: (5 kHz range)	215-225			7.9
	125-150			7.9
	95			3.1
	45			2.4
	1375			1.8
Bottom bearing housing				
Accelerations: (10 kHz range)	4000-6000	6	15	15
	1875-1900	2	13	20
	1475-1575	3	21	25
	1100-1200	4	32	35
	950-1050	7	50	40
	770-850	4	32	32
	525-575	7	38	45
	420-430	4	31	25
	270-330	8	8	30
	215-225	3	35	27
	125-150	4	29	30
	95	3	10	10
Velocities: (5 kHz range)	220 → 230			6.5
	120 → 140			10.5
	95			4.3
	85			3.0
	6 → 14			17.2

Table 7.7 Principal frequencies of the resonances generated by LEROS during a *high* speed test, measured as accelerations and velocities. Disc surface undulation frequencies are shown.

VIBRATION MONITORING OF A LOW SPEED TEST

Test 52: BS11 rail steel top disc, Type 'D' tyre bottom disc, maximum contact stress 500 MPa, creepage 10%, test length 10^5 top disc revolutions.

	Load (N)	Top disc speed (rpm)	(Hz)	Bottom disc speed (rpm)	(Hz)
Test start:	801	88.40	1.47	97.69	1.63
Test end :	790	88.25	1.47	97.35	1.62

At each weighing interval, the load and DC motor speeds were trimmed so as to maintain constant contact stress and creepage with respect to the different worn diameters of the test discs and slight variations in Lathe speed.

Frequencies and maximum amplitudes of facets that formed on the worn disc surfaces:

	Top disc		Bottom disc
Frequencies at 60,000 revs.	Half circumference	≃ 70.6 Hz	No facets
	Half circumference	Not distinct	
Max. amplitude :	± 4.5 μm		
Frequencies at 100,000 revs.	Half circumference	≃ 61.8 Hz	No facets
	Half circumference	Not distinct	
Max. amplitude :	± 4.5 μm		

Transducer location	Principal Frequencies (Hz)	Signal strength (mV) (Top disc revs X1000) ≃3	≃60	≃100
Top bearing housing				
Accelerations:	5800-6000	30	16	4
(10 kHz range)	5400 → 6100	>15	>6	>3
	4750	2	2	12
	2375	8	8	9
	1785	1.8	2.1	2.5
	1150	3.8	2.5	2.7
	670	2.0	1.8	2.1
	300	2.2	2.4	2.3
	40-45	3.3	3.7	3.2
Velocities:	100-101		0.4	0.4
(2 kHz range)	67-68		0.4	0.4
	40-45		2.8	2.5
	27.5		0.7	0.8
	18.5		0.6	0.6
Bottom bearing housing				
Accelerations:	5500-5700	16	9	
	5350			6
(10 kHz range)	5300 → 6000	>6	>5	
	4600 → 5500			>2.4
	1150	2.7	2.9	5.2
	300	2.6	2.4	2.8
	40-45	2.4	2.4	2.2
Velocities:	112-113		0.6	0.2
(5 kHz range)	100-101		0.4	0.3
	67-68		0.2	0.2
	40-45		1.7	1.4
	27.5		0.6	0.6
	18.5		0.5	0.7

Table 7.8 Principal frequencies of resonances generated by LEROS during a *low* speed test, measured as accelerations and velocities. Disc surface undulation frequencies are shown.

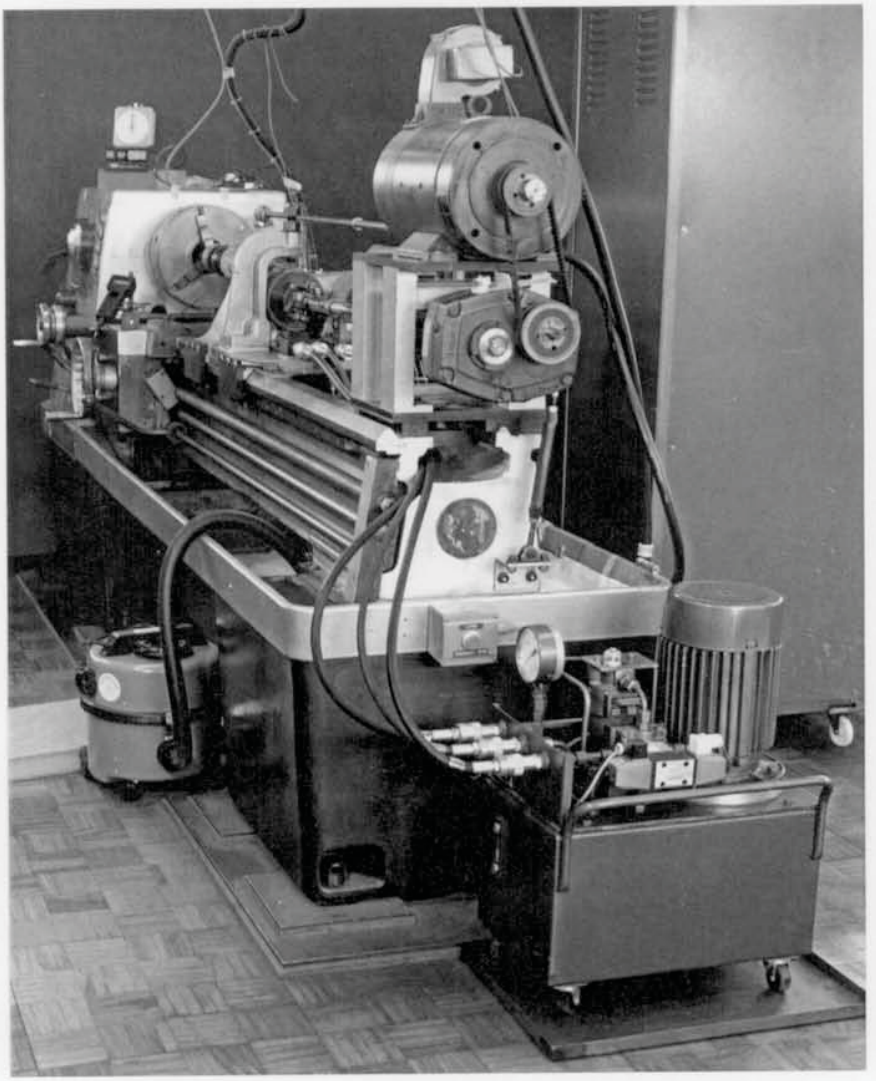

Figure 7.1 An overview of LEROS. To the foreground, the hydraulic power pack and the DC motor and gearing which drive the bottom disc. To the left, the vacuum extraction for the environment chamber. [Note: In this photographic figure and those following, the safety cage was removed for access.]

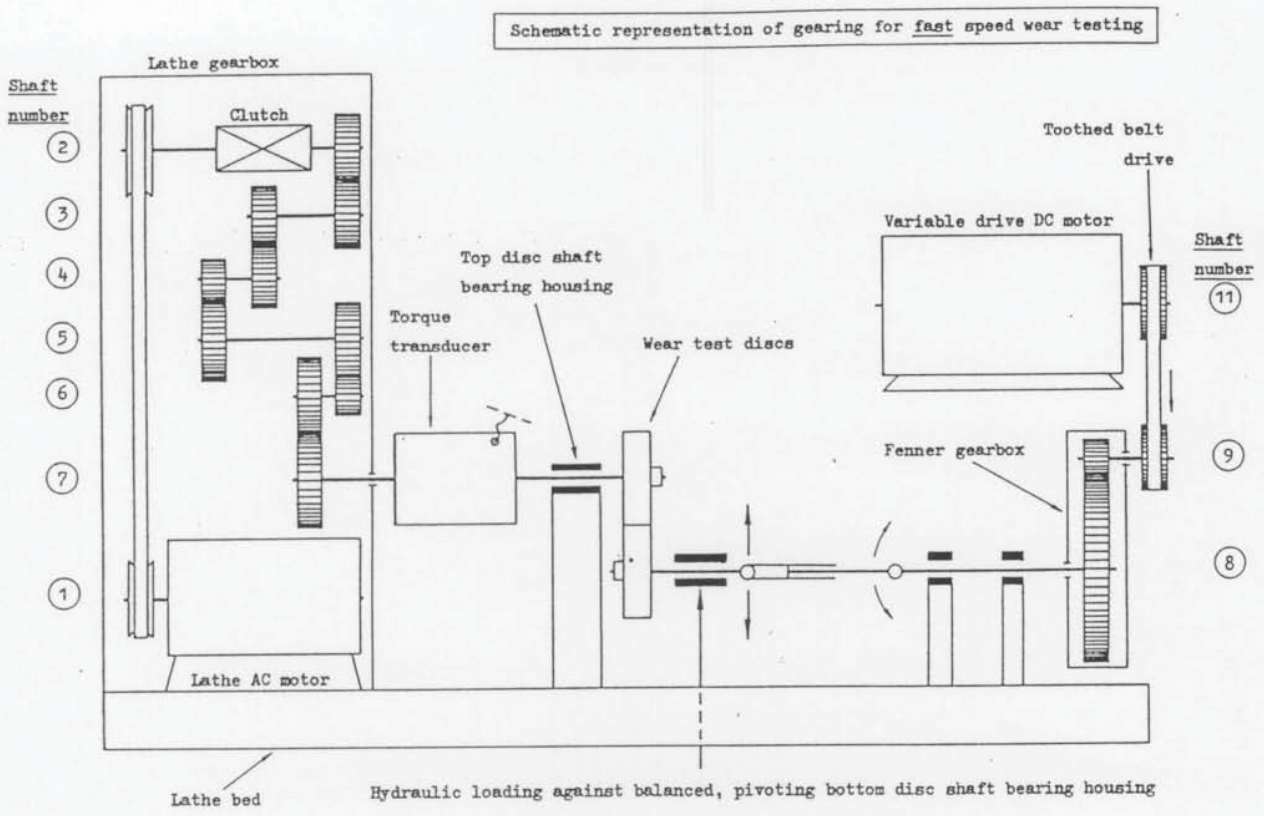

Lathe (top shaft) gearing set at "370 rpm" and 4.287:1 Fenner gear used between the DC motor and the bottom shaft.

SHAFT		ROTATIONAL SPEED rpm	Hz	NUMBER OF GEAR TEETH	GEAR TOOTH IMPACT FREQ. Hz
1	Lathe motor	1518	25.29	'V' pulley	-
2	Clutch shaft	1117	18.62	'V' pulley	-
				36	670
3	Drive shaft	1117	18.62	36	670
				31	577
4	Second shaft	962	16.03	36	577
				18	289
5	Inter-shaft	385	6.41	45	289
				37	237
6	Idler shaft, free running on Second Shaft	593	9.89	24	237
				46	455
7	Spindle, TOP DISC	401.3	6.69	68	455
		For 10% creepage			
8	BOTTOM DISC shaft	443.5	7.39	112	828
9	First Fenner shaft	2258	37.63	22	828
				32	1204
10	No second shaft in this gearbox				
11	DC Motor	1901	31.69	38	1204
		For 3% creepage			
8	BOTTOM DISC shaft	413.5	6.89	112	772
9	First Fenner shaft	2105	35.08	22	772
				32	1123
11	DC Motor	1773	29.54	38	1123

Figure 7.2 A schematic view of LEROS as set for *high* speed testing, showing the gearing arrangement and listing gear impact frequencies.

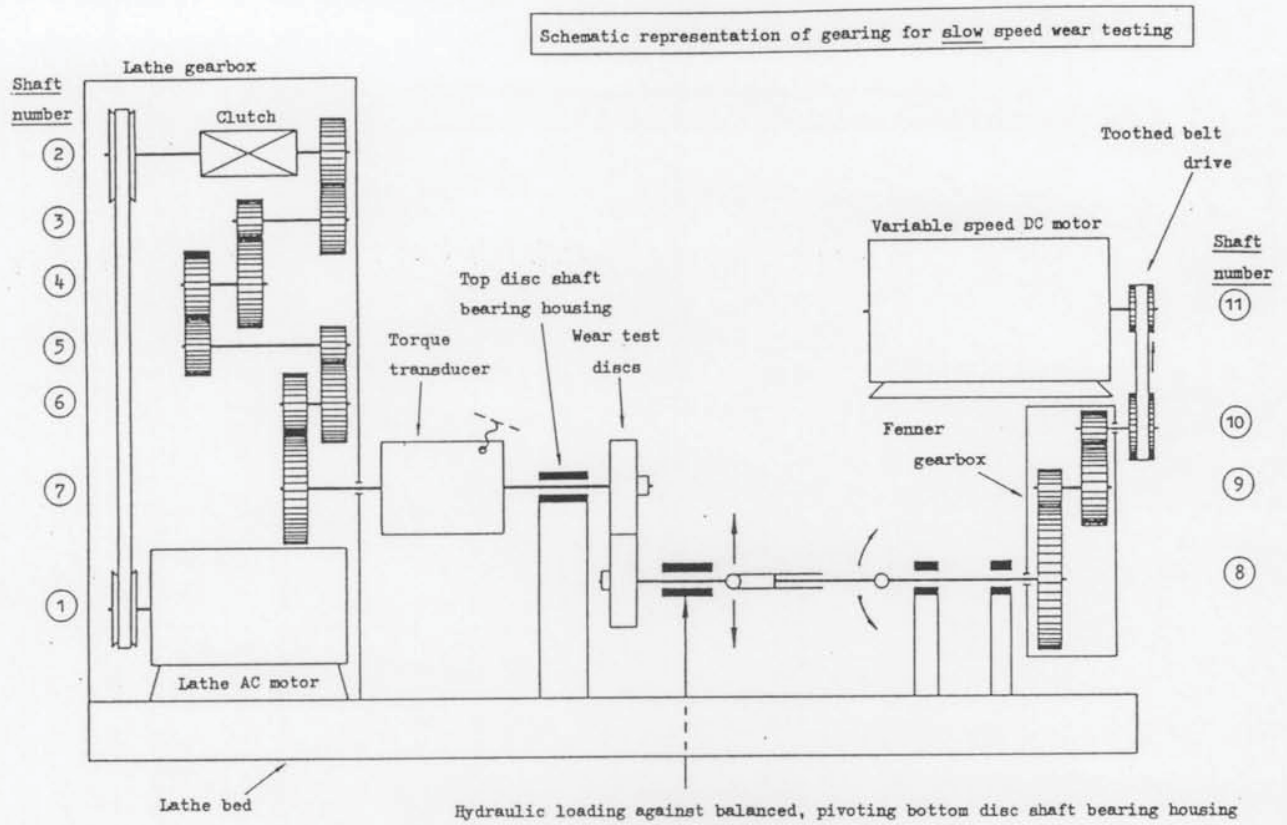

Lathe (top shaft) gearing set at "87 rpm" and 17:1 Fenner gear used between the DC motor and the bottom shaft.

SHAFT		ROTATIONAL SPEED rpm	Hz	NUMBER OF GEAR TEETH	GEAR TOOTH IMPACT FREQ. Hz
1	Lathe motor	1518	25.29	'V' pulley	-
2	Clutch shaft	1117	18.62	'V' pulley	-
				36	670
3	Drive shaft	1117	18.62	36	670
				26	484
4	Second shaft	708	11.81	41	484
				35	413
5	Inter-shaft	886	14.76	28	413
				17	251
6	Idler shaft, free running on Second Shaft	327	5.45	46	251
				24	131
7	Spindle, TOP DISC	88.25	1.47	89	131
		For 10% creepage			
8	BOTTOM DISC shaft	97.54	1.63	101	164
9	First Fenner shaft	493	8.21	20	164
				70	575
10	Second Fenner shaft	1326	22.10	26	575
				40	884
11	DC Motor	1658	27.63	32	884
		For 3% creepage			
8	BOTTOM DISC shaft	90.94	1.52	101	153
9	First Fenner shaft	459	7.65	20	153
				70	536
10	Second Fenner shaft	1236	20.61	26	536
				40	824
11	DC Motor	1546	25.76	32	824

Figure 7.3 A schematic view of LEROS as set for *low* speed testing, showing the gearing arrangement and listing gear impact frequencies.

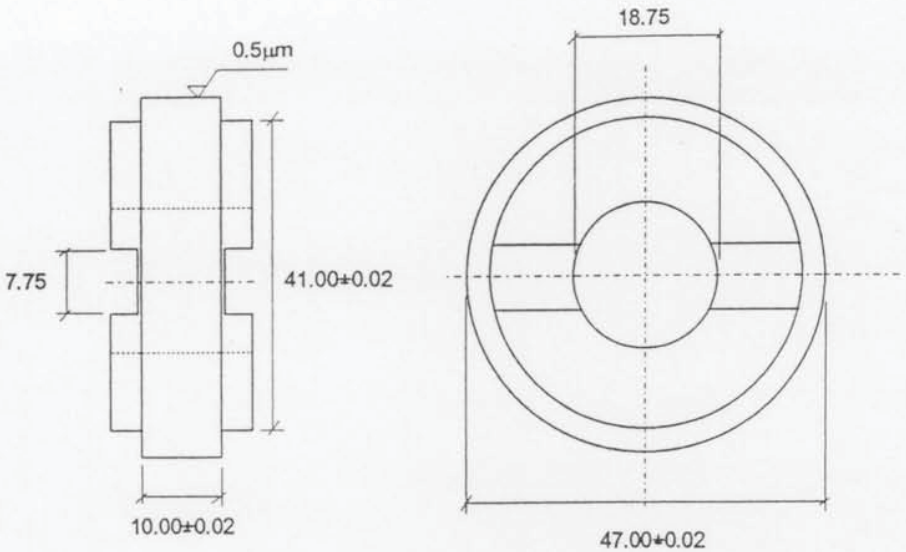

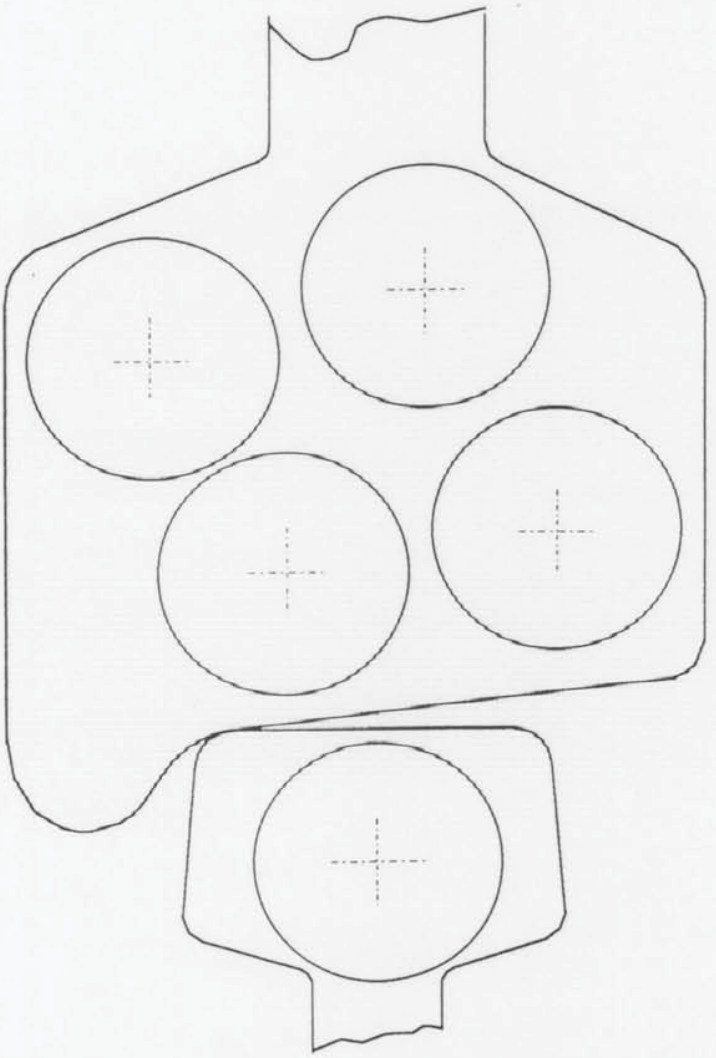

Figure 7.4 LEROS test disc dimensions and disc locations within rail and wheel tyre sections[drawing from Tyfour et al, 1995]

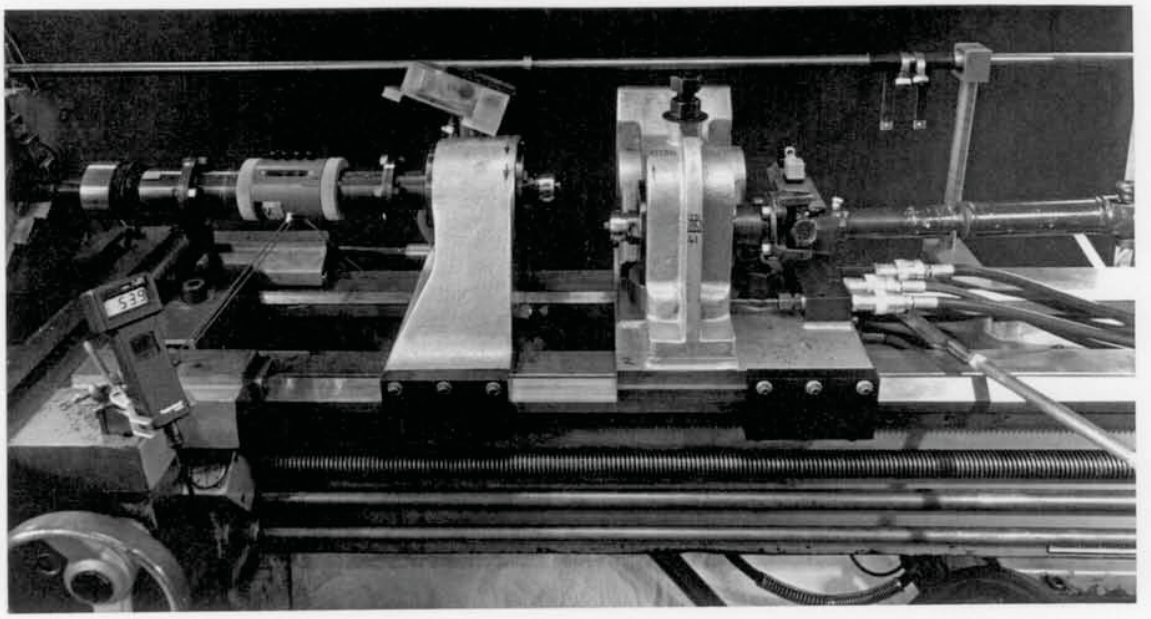

Figure 7.5 LEROS ready for disc loading. Once loaded, the bottom disc bearing assembly can be slid left against an adjustable stop so that wear tracks are precisely aligned. The torque transducer is located to the left of the top bearing housing. The drive bar in the lathe chuck is pinned to ensure that no slippage occurs.

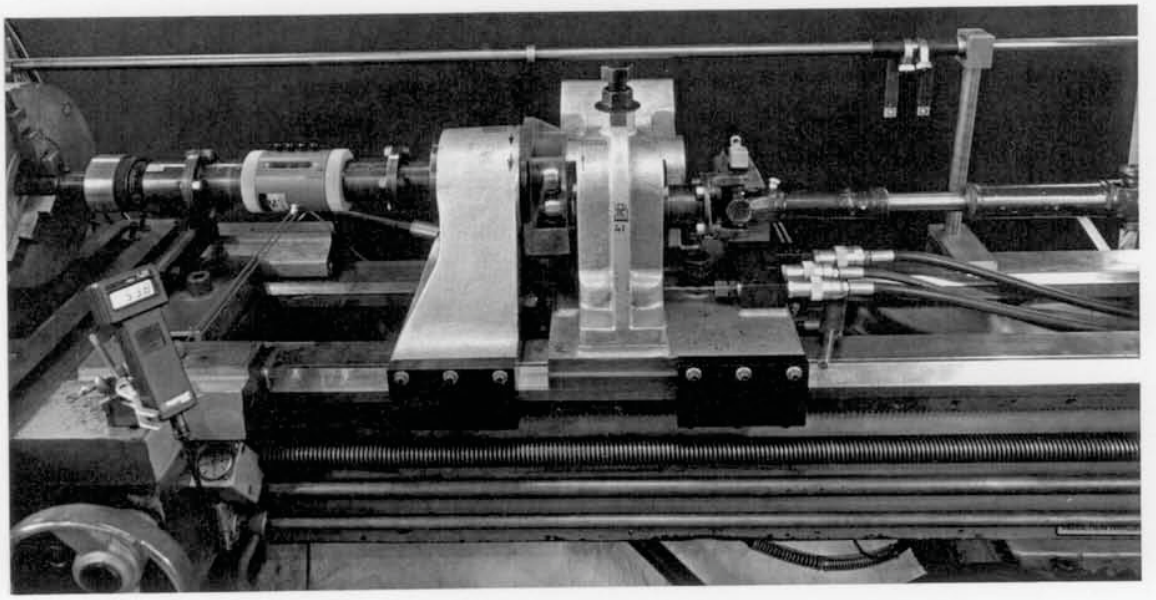

Figure 7.6 LEROS set ready for testing with discs enclosed in the environment chamber. The instrument in the foreground is showing environment chamber humidity.

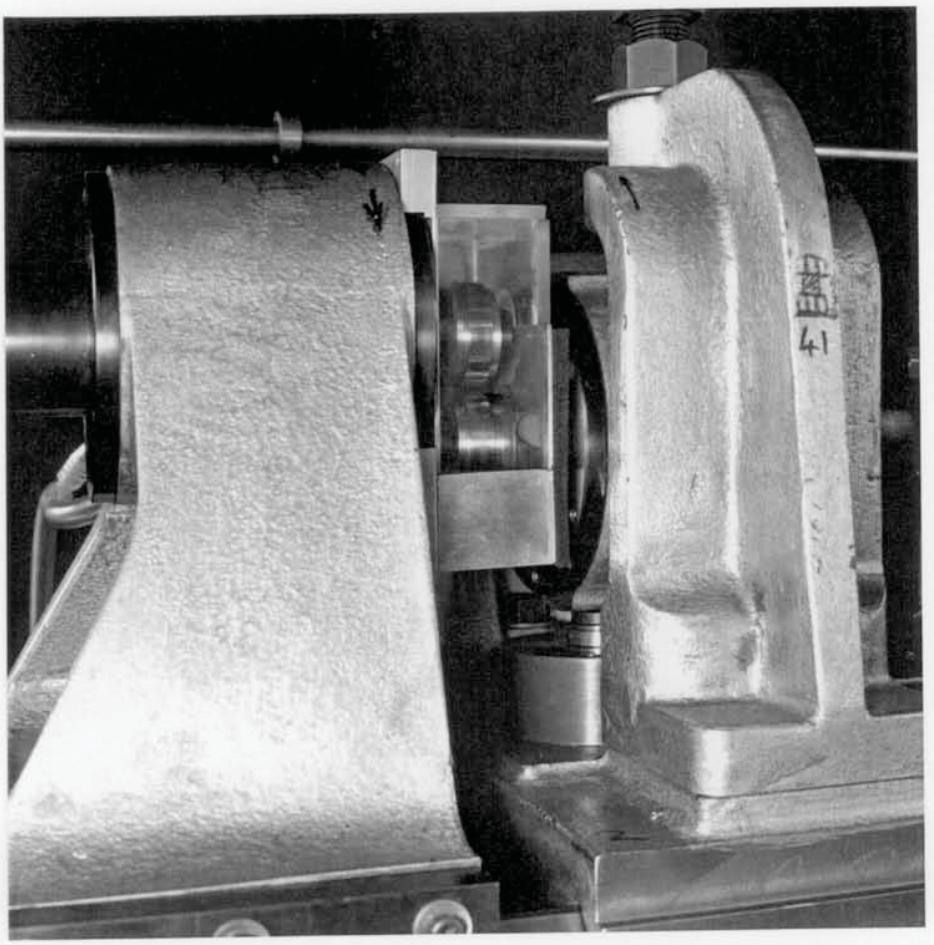

Figure 7.7 The bottom disc bearing housing pivoted up and loaded by the hydraulic ram.

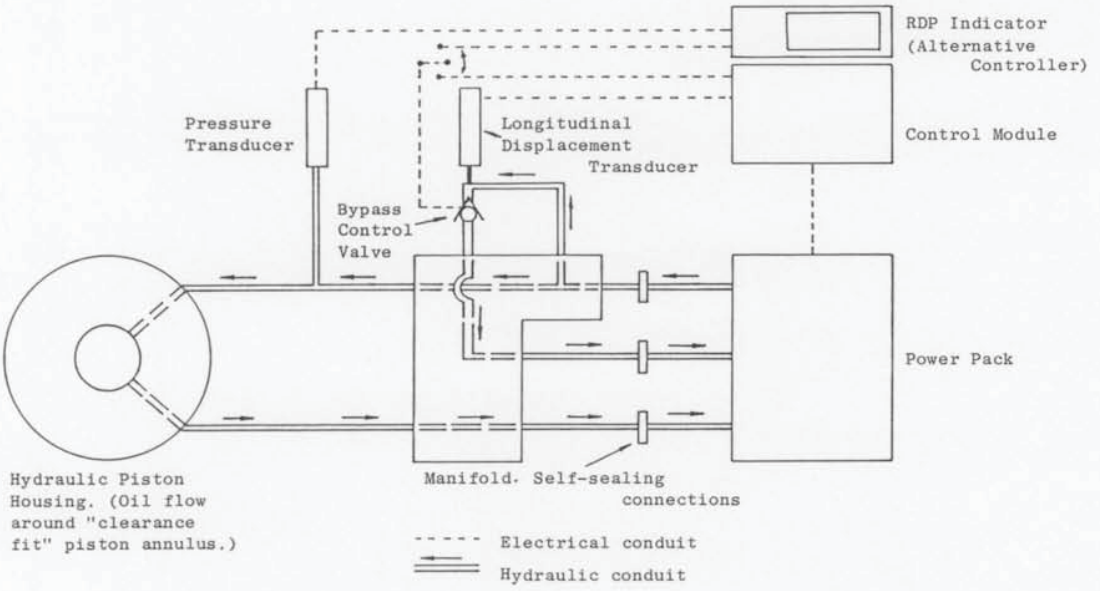

Figure 7.8 A schematic of the hydraulic loading system.

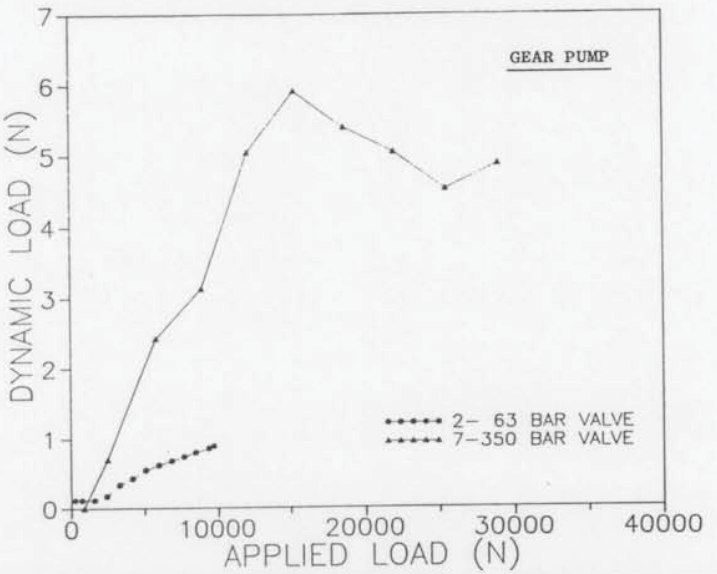

The maximum dynamic loads generated during calibration trials of the hydraulic loading system, using two types of pump in the power pack.

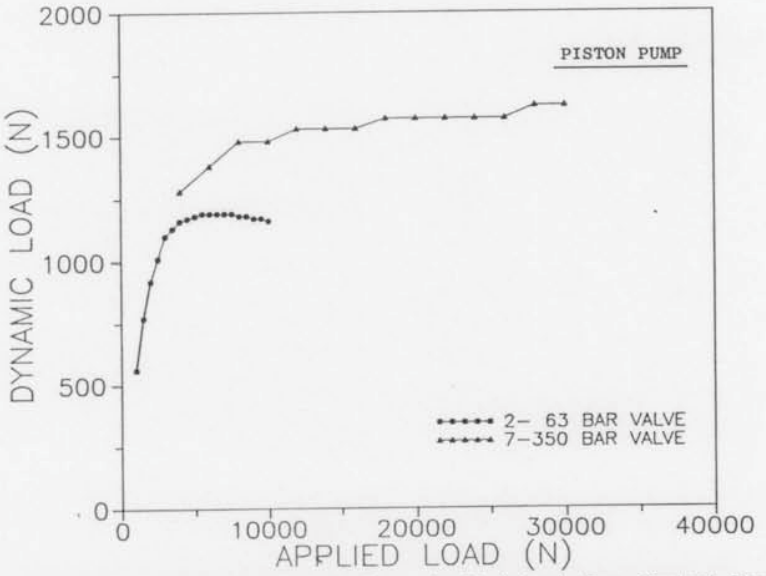

NOTE. For standard sized test discs:

Applied Load	Max. Contact Stress
801 N	500 MPa
3875 N	1100 MPa
10376 N	1800 MPa

Figure 7.9 Two orders of magnitude reduction in hydraulic load pulsing amplitude achieved by replacement of the (power pack) piston pump with a gear pump.

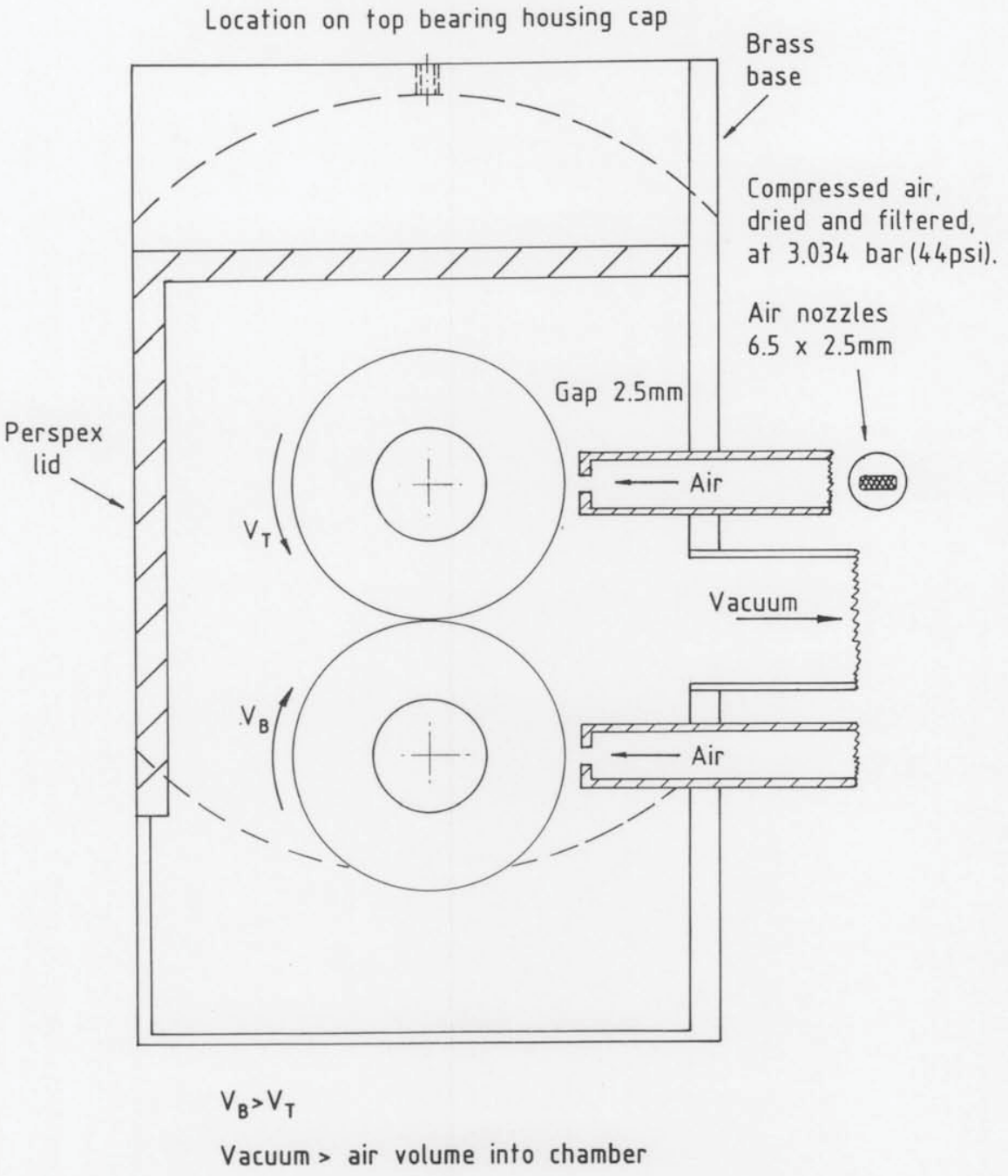

Figure 7.10 The design of the LEROS environment chamber.

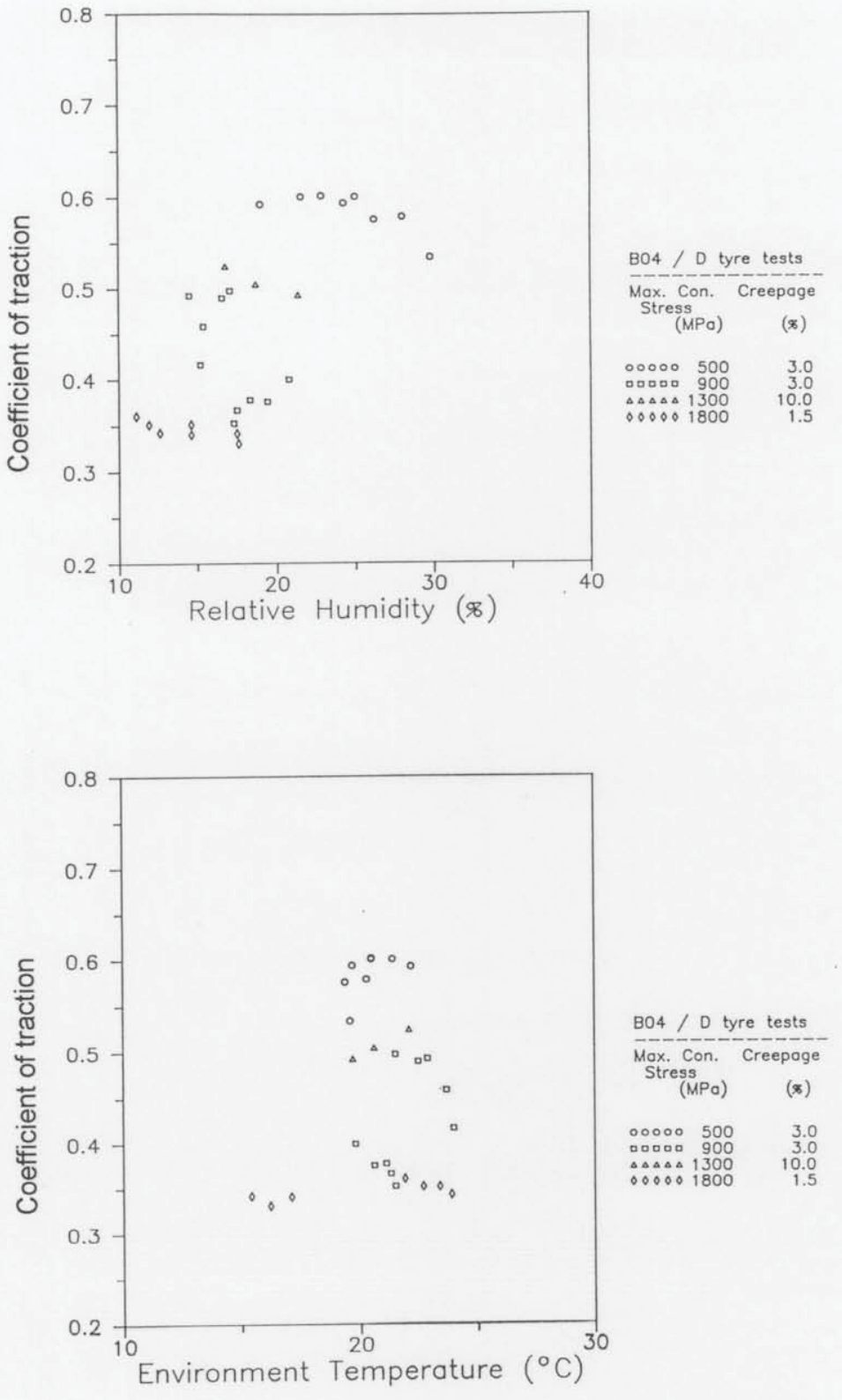

Figure 7.11 The relationships between coefficient of traction and environment chamber conditions for B04 / W64 tests.

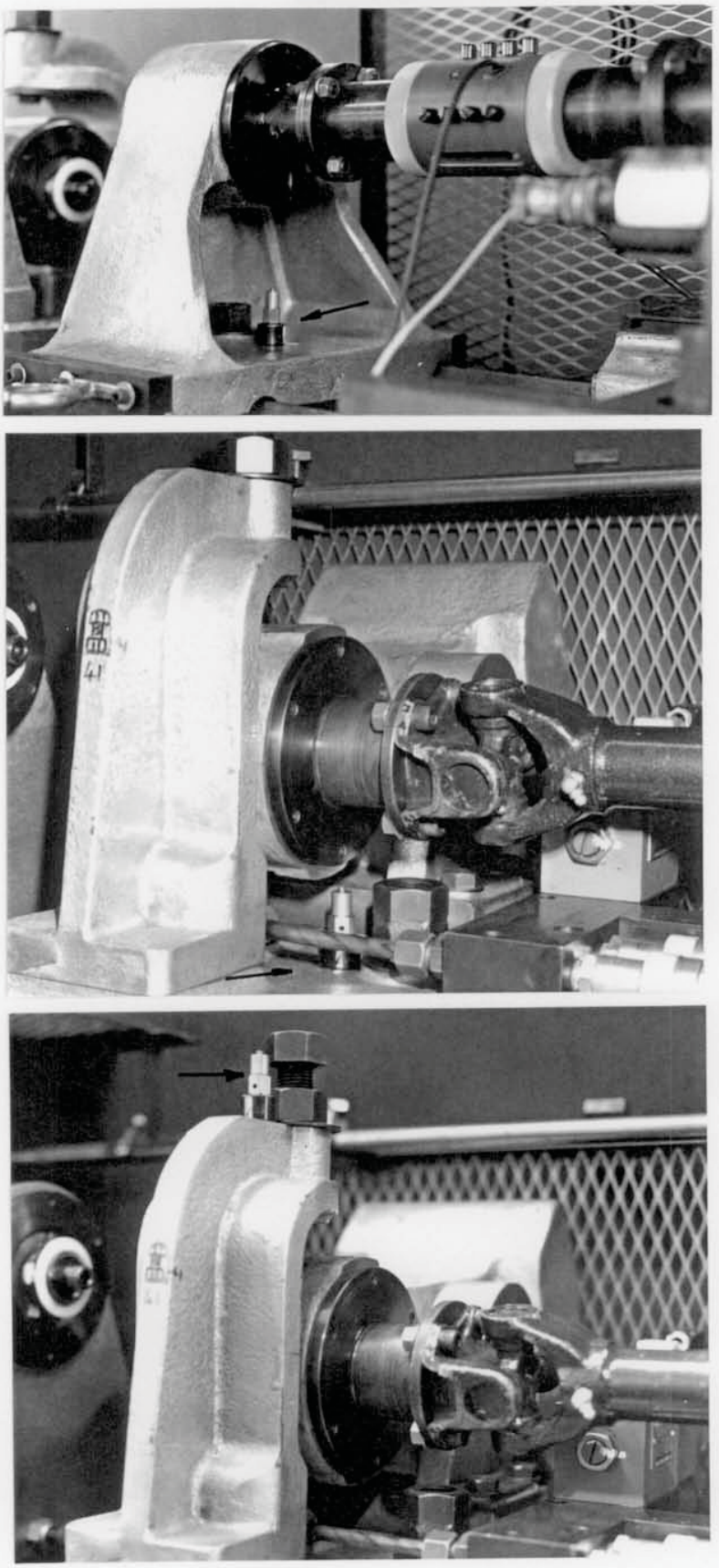

Figure 7.12 Location of the accelerometer used for vibration analysis. (a) Top disc bearing housing location. (b) Bottom disc bearing housing location. (c) Location next to safety bolt for measuring hydraulic loading vibrations.

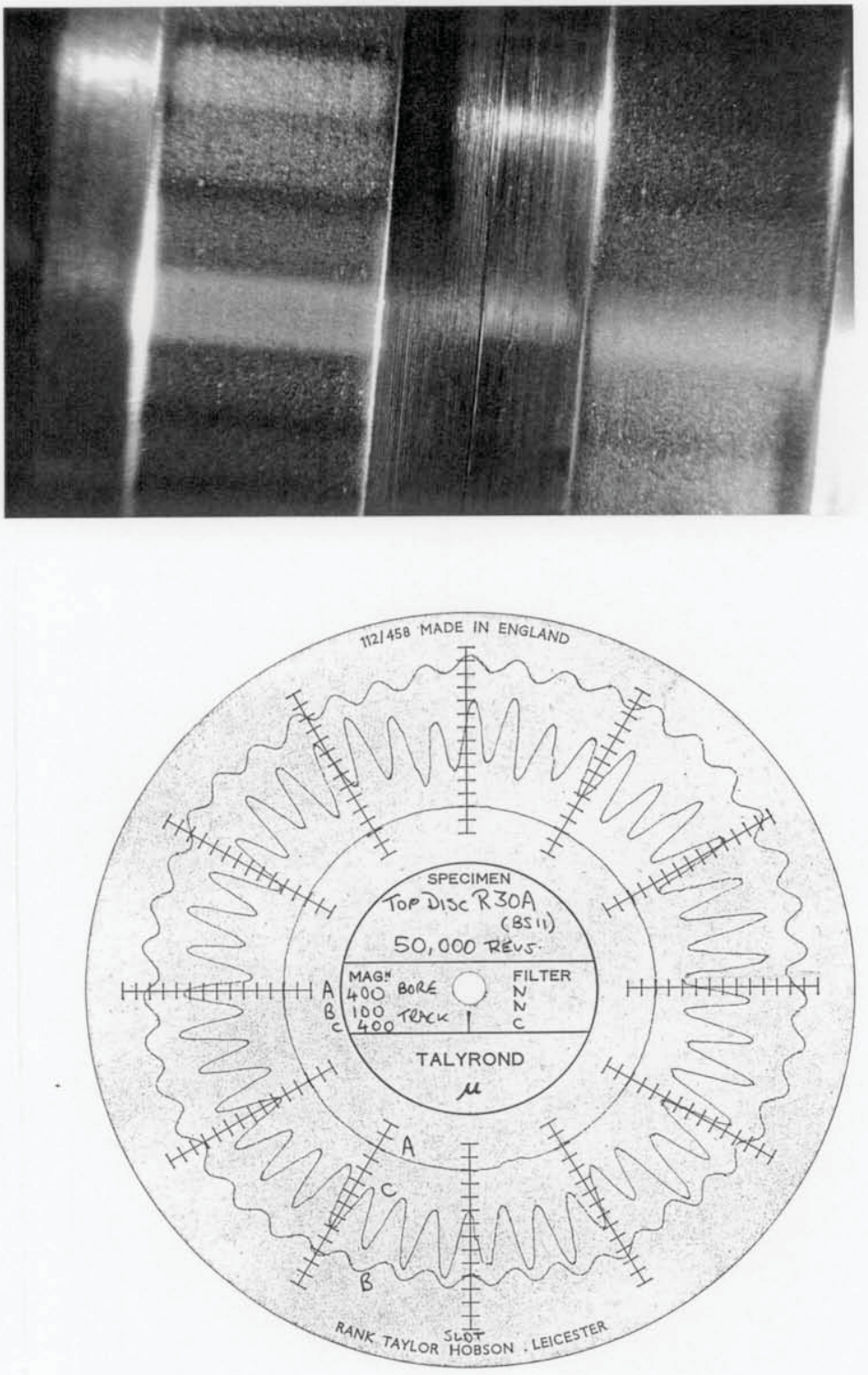

Figure 7.13 A faceted R52 top disc (left, above) and its Talyrond profile. (Test 30A, 900 MPa p_o, 7% creepage, after 50K revs.)

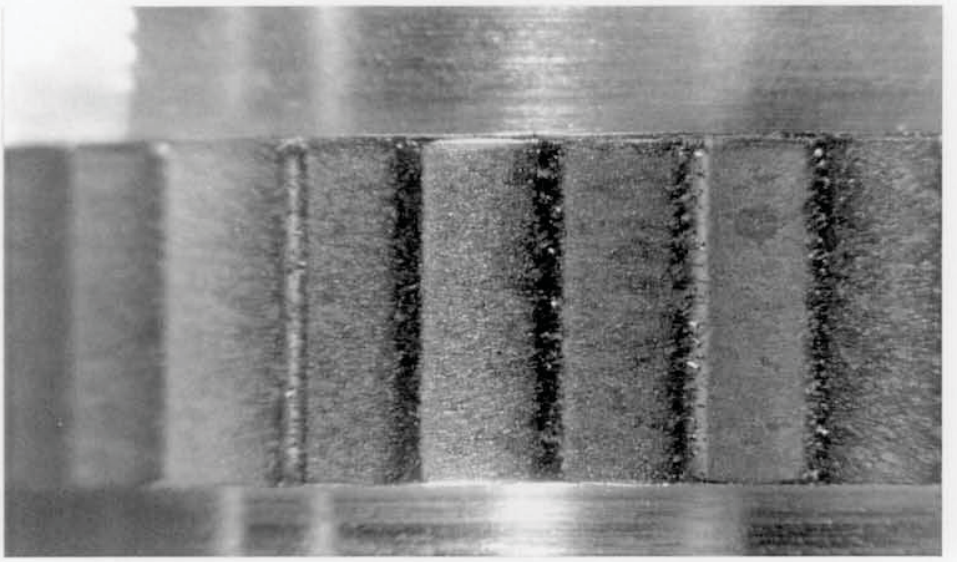

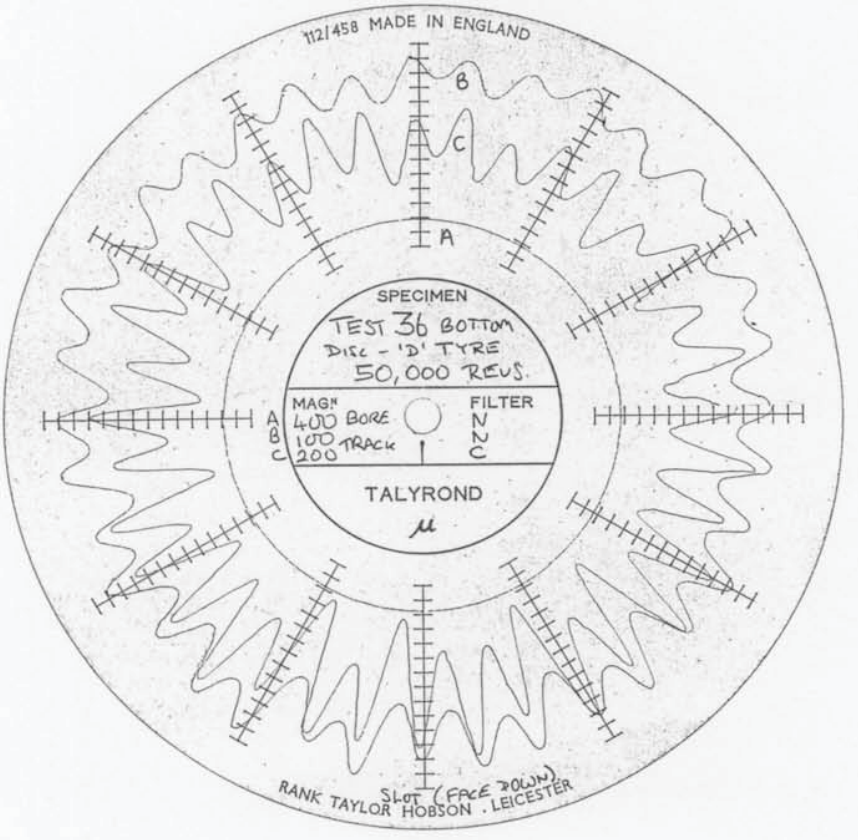

Figure 7.14 A W64 bottom disc with clear facets at the mid-test stage* (*50K top disc revs.) and its Talyrond profile. (Test 36, B04 top disc, 900 MPa p_o, 3% creepage. Rolling and sliding from left to right.)

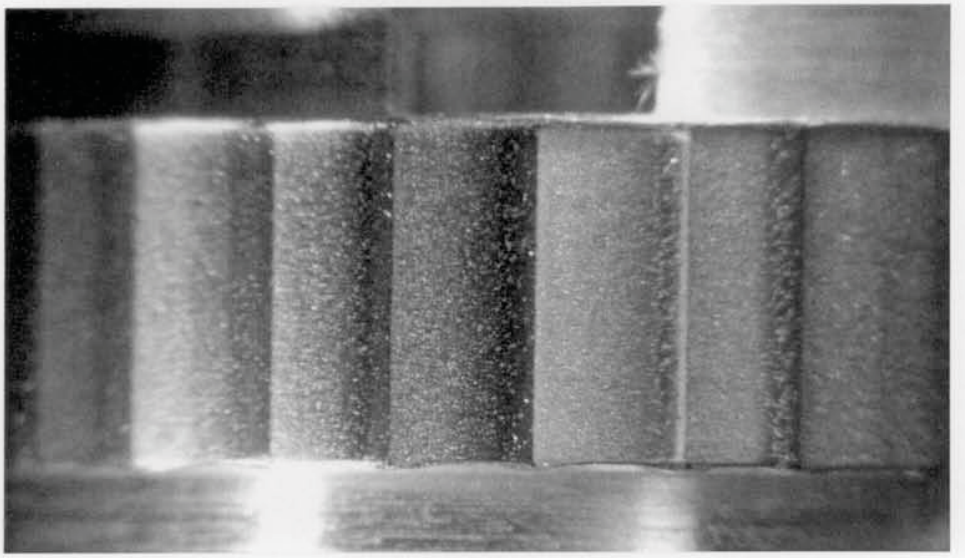

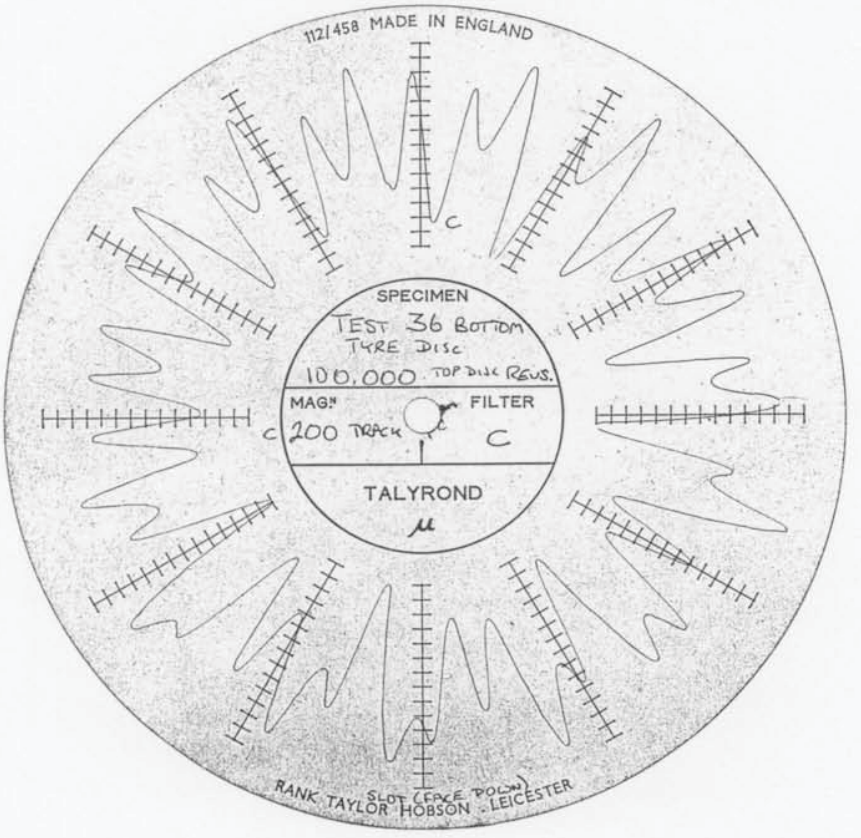

Figure 7.15 The disc shown in the previous figure at the test end (100K top disc revs) and its Talyrond profile. Some double facet peaks have formed.

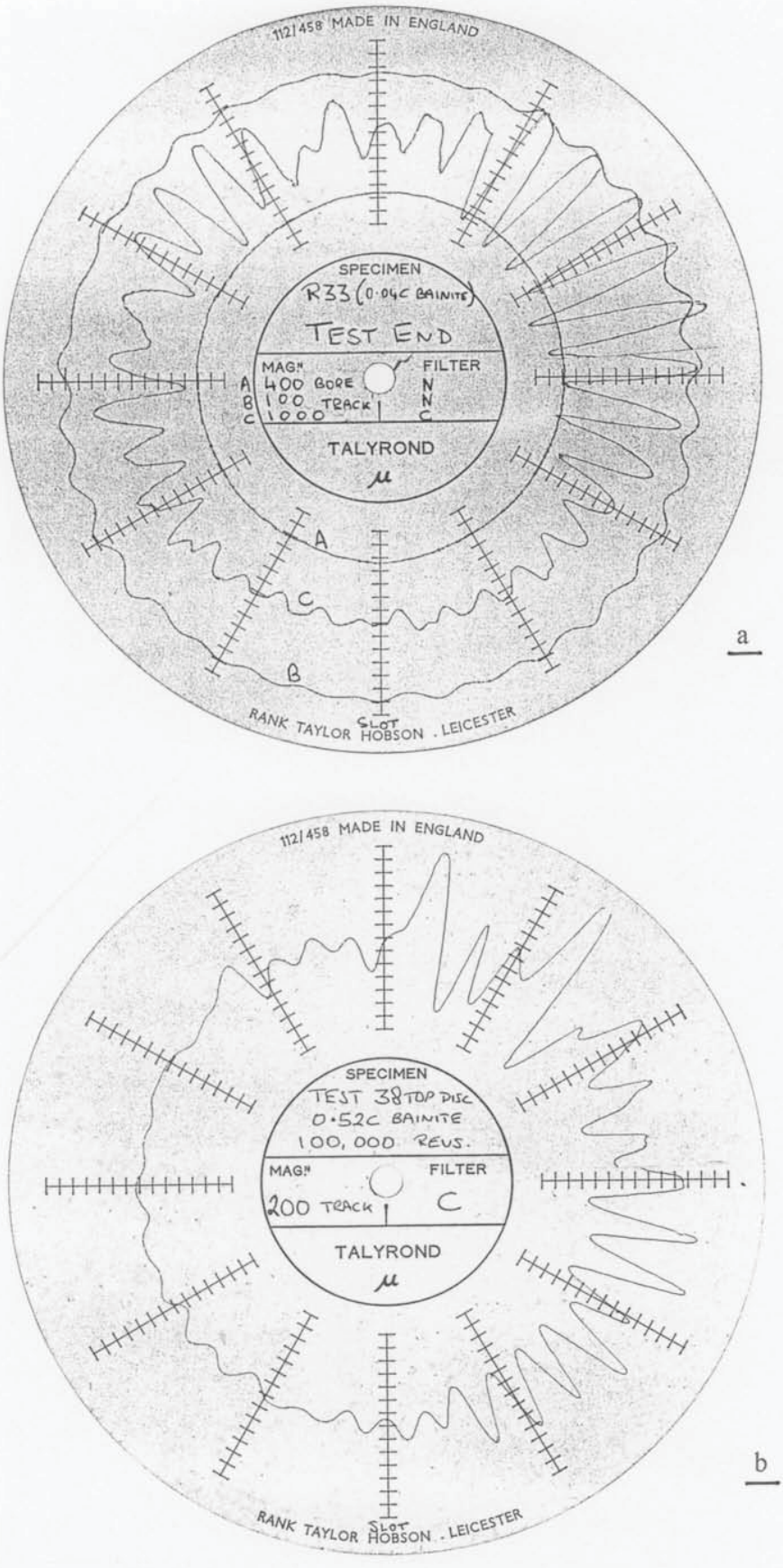

Figure 7.16 Top disk Talyrond profiles showing asymmetric patterns. (a) Asymmetric facet amplitudes (Test 33 B04 top disc, 500 MPa p_o, 3% creepage). (b) Asymmetric amplitudes and wavelengths (Test 38 B52 top disc, 900 MPa p_o, 3% creepage).

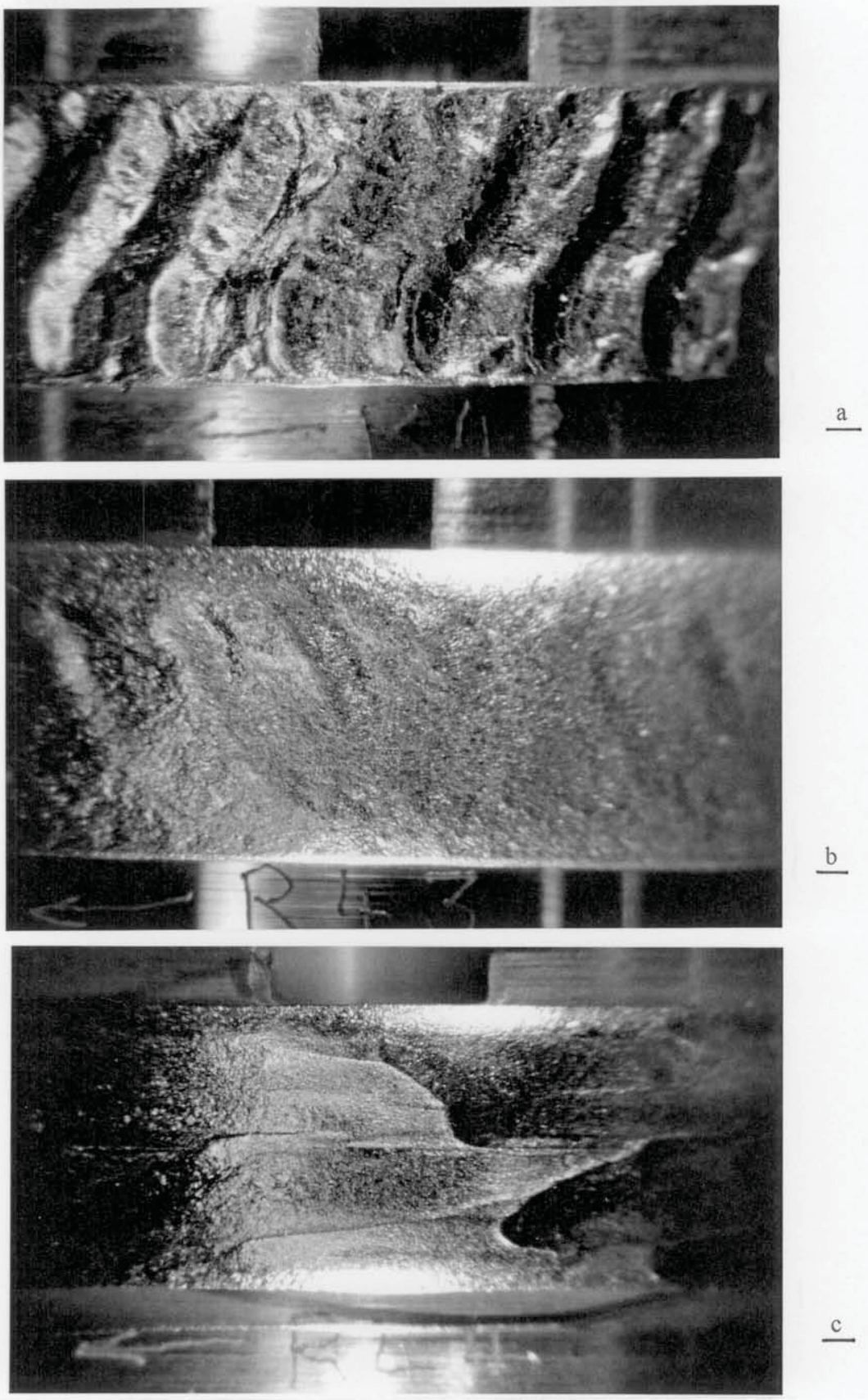

Figure 7.17 Ripple formation on top disks tested at 1300 MPa p_o and 10% creepage. (Rolling from left to right; sliding in opposite direction.) (a) Test 42 R52 disc after 5K revs. (b) Test 43 B04 disc after 7.5K revs. (c) Test 44 B20 disc after 10K revs.

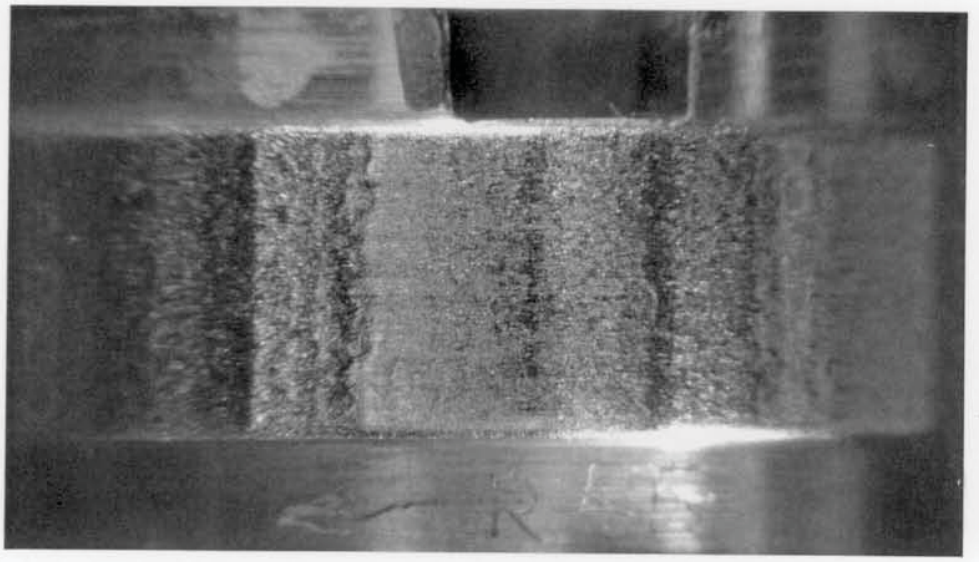

a

b

Figure 7.18 The change in wear pattern of the B52 top disc tested at 1300 MPa p_o, 10% creepage (Test 45 - rolling from left to right, sliding in opposite direction). (a) Faceted after 5K revs. (b) Rippled after 7.5K revs.

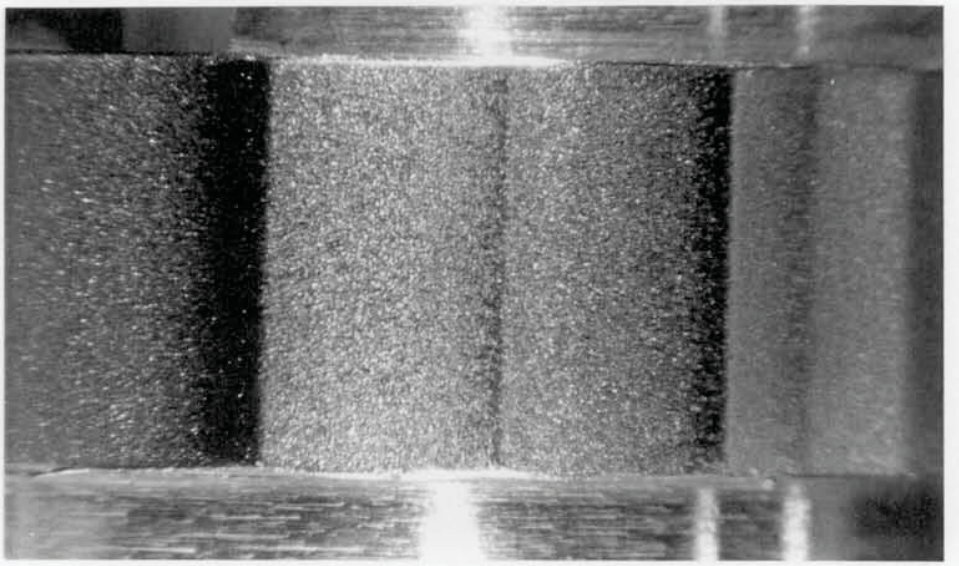

a

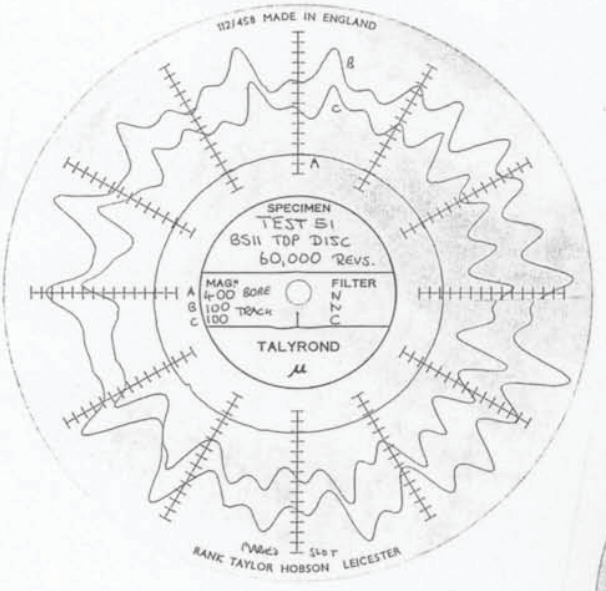

b

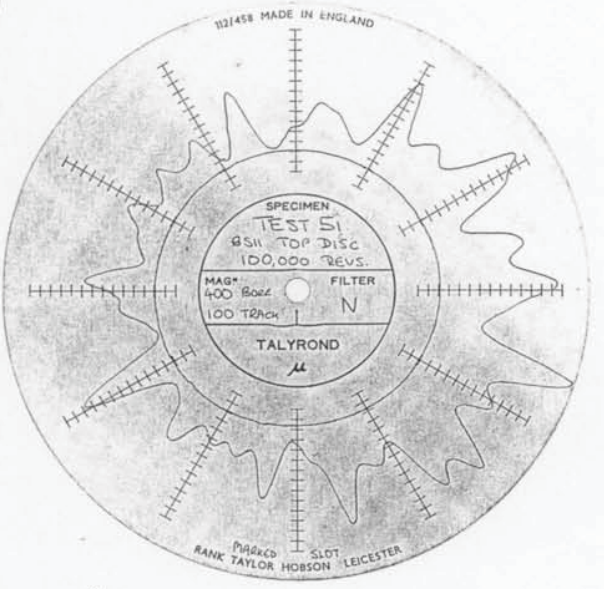

c

Figure 7.19 The R52 top disc from the high speed test used for vibration analysis (Test 51, 500 MPa p_o, 10% creepage; rolling from right to left, sliding in opposite direction). (a) Uneven facet features after 100K revs. (b) Facet pattern on Talyrond profile after 60K revs. (c) Far more uneven profile after 100K revs.

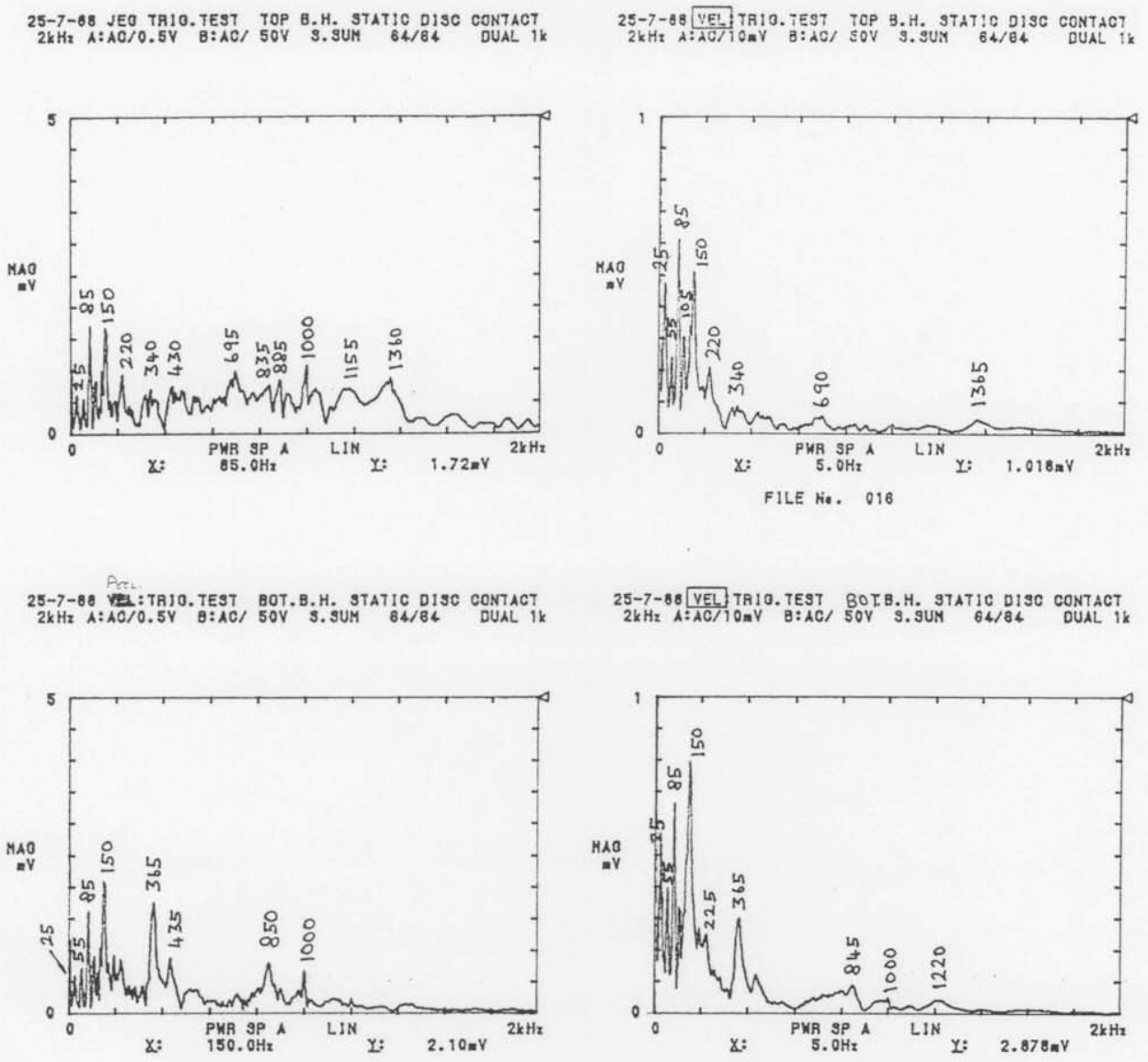

Figure 7.20 Frequency spectra of natural resonances generated by vibrating LEROS whilst static. Accelerations are shown on the leftside and velocities on the rightside, for the top bearing housing (top figures) and the bottom bearing housing (bottom figures).

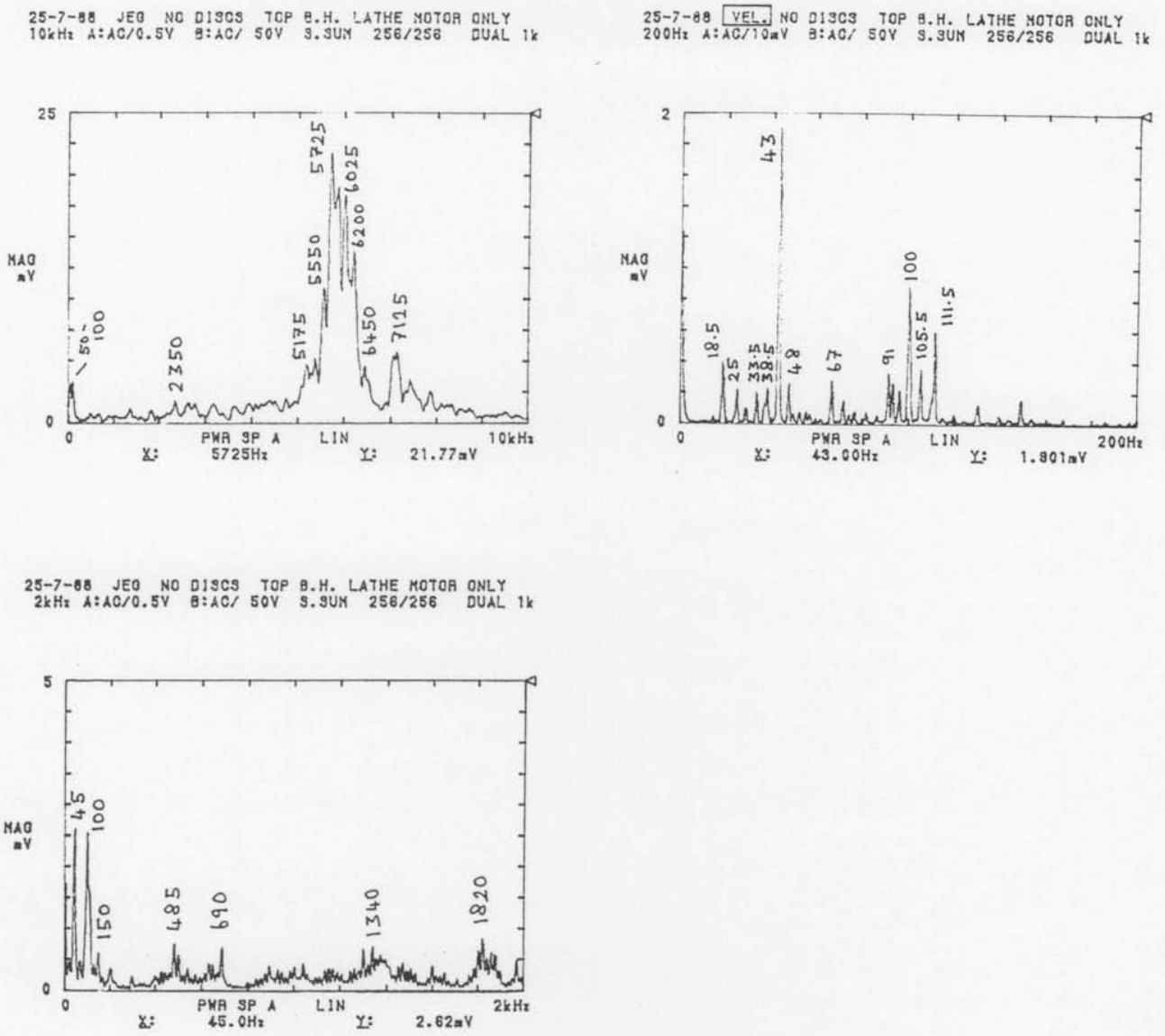

Figure 7.21 Frequency spectra of vibrations generated by the idling lathe AC motor of LEROS (including pulleys and clutch layshaft); all other gearing static. All measurements on the top bearing housing; two frequency axes are shown with accelerations on the leftside; velocities shown on the rightside.

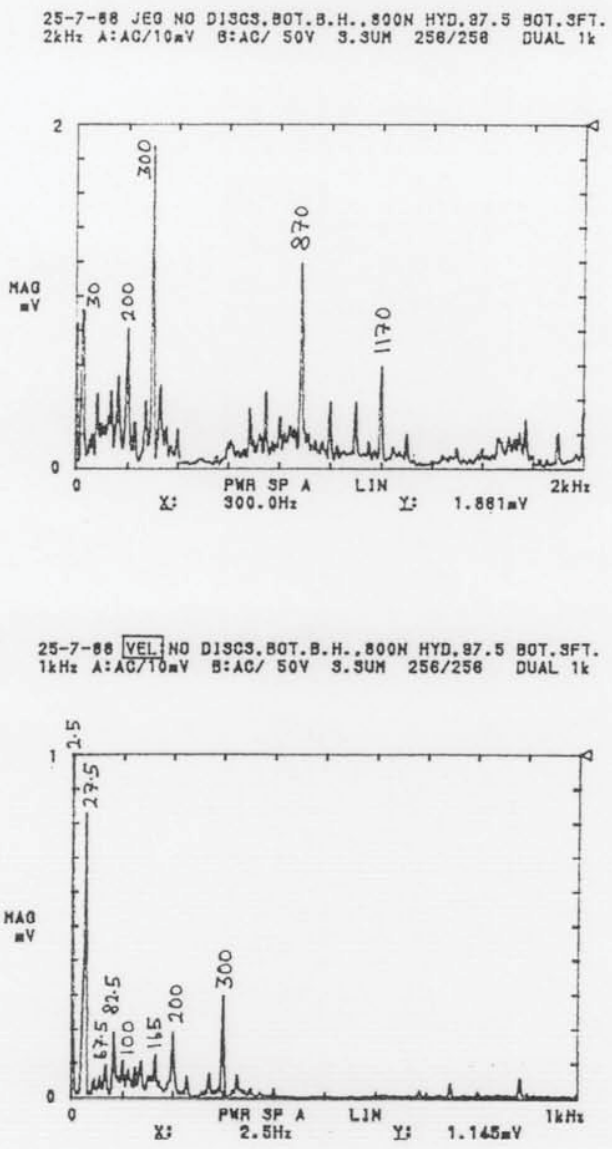

Figure 7.22 Frequency spectra of vibrations generated on LEROS with only the hydraulic loading operative; measured next to the safety bolt. Top - accelerations, bottom - velocities.

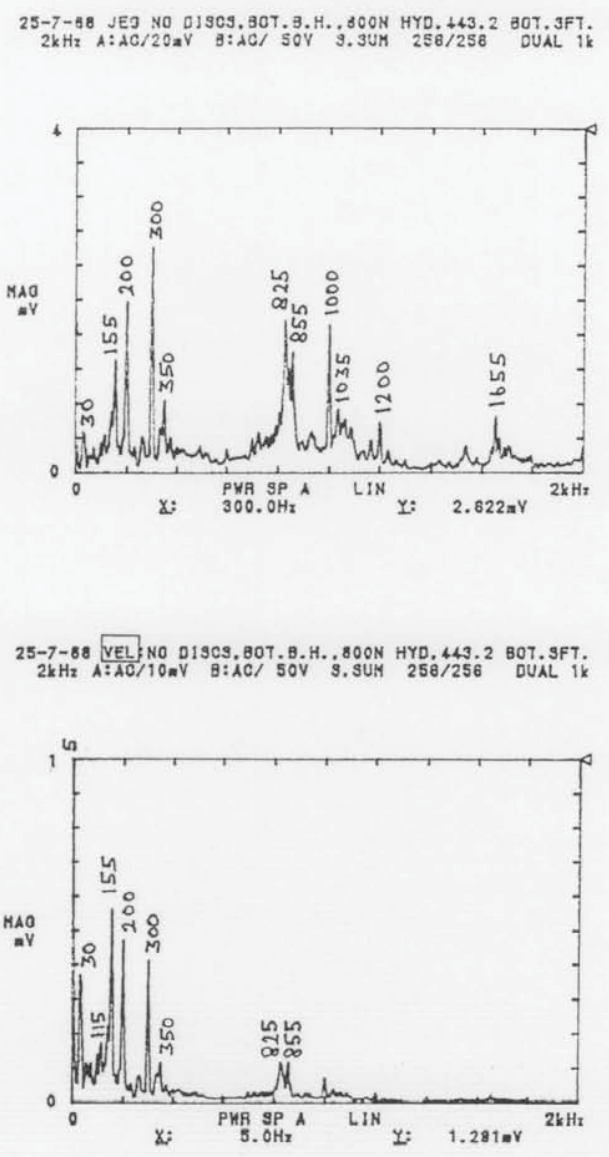

Figure 7.23 Frequency spectra of vibrations generated on LEROS with the bottom disc bearing housing hydraulically loaded against the safety bolt together with the bottom drive operating at the higher speed setting. Measured on the bottom bearing housing. Top - accelerations, bottom - velocities.

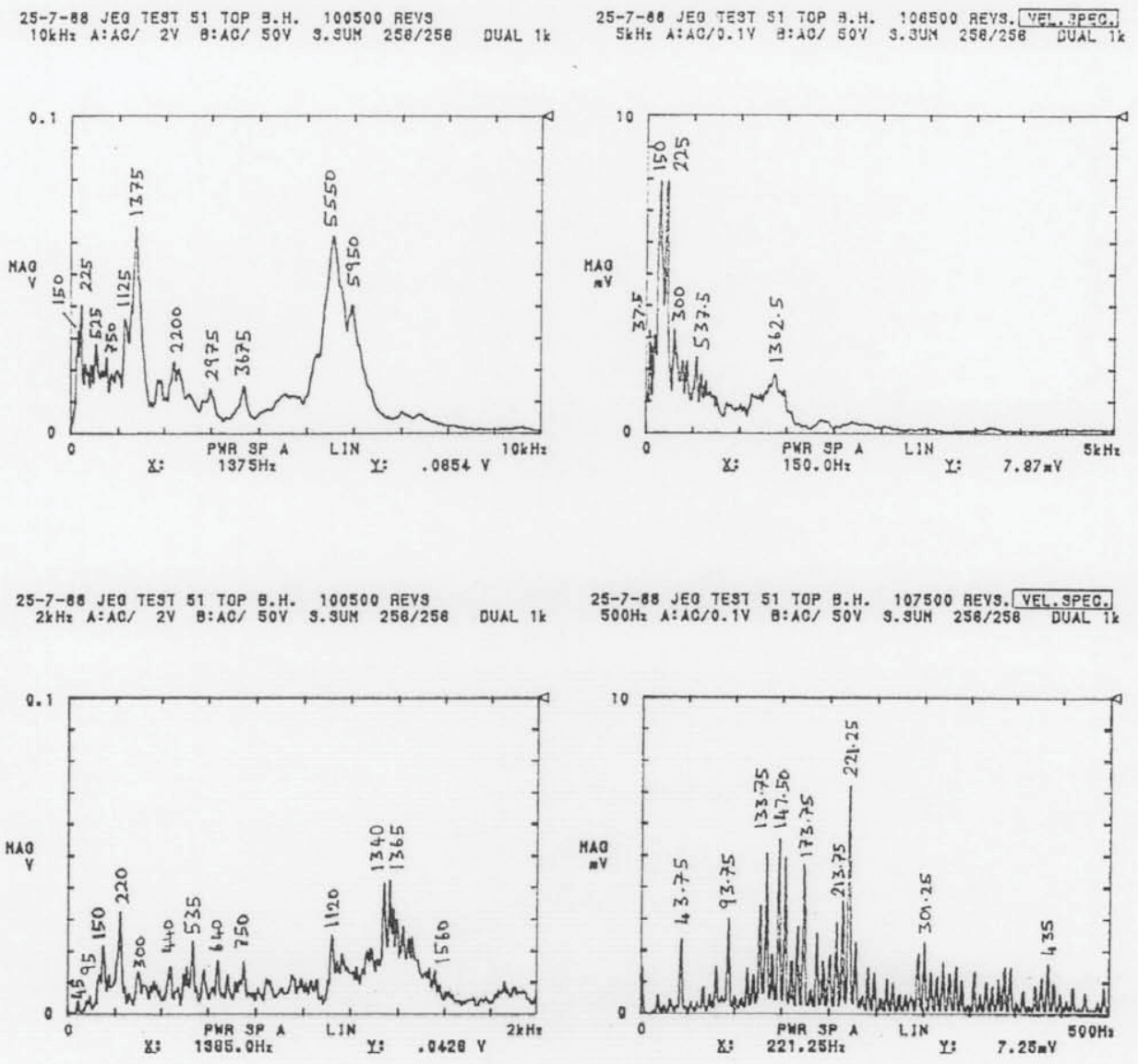

Figure 7.24 Frequency spectra of vibrations generated on LEROS at the top bearing housing at the end of a high speed test (Test 51). Leftside - accelerations on two frequency range axes; rightside - respective velocities.

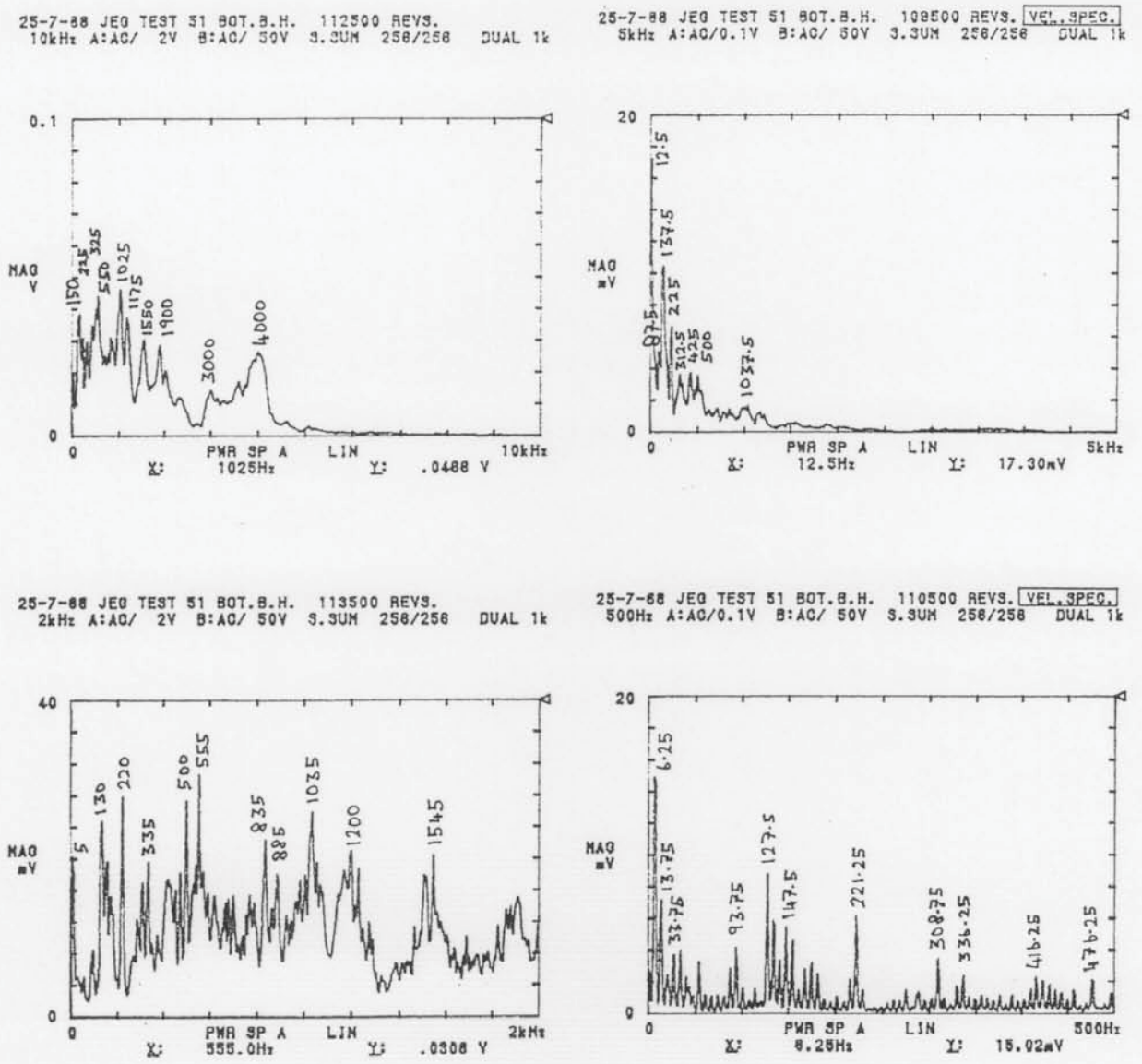

Figure 7.25 Frequency spectra of vibrations generated on LEROS at the bottom bearing housing at the end of a high speed test (Test 51). Leftside - accelerations on two frequency range axes; rightside - respective velocities.

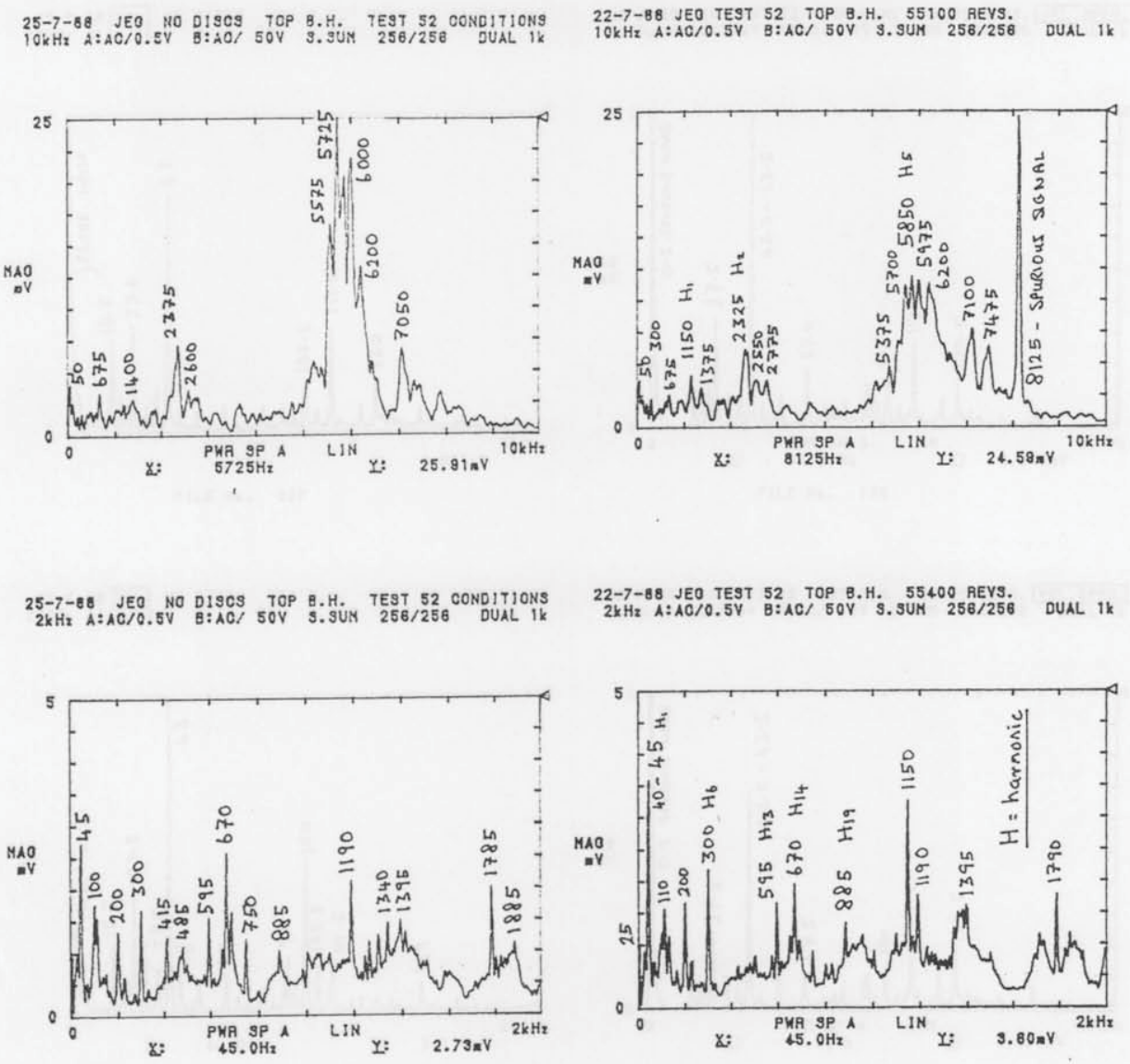

Figure 7.26 Comparative frequency spectra of accelerations generated on LEROS, measured on the top bearing housing, with the machine running empty at low speed (leftside, shown on two frequency range axes) and mid-way through the low speed test (Test 52; shown rightside on two frequency ranges).

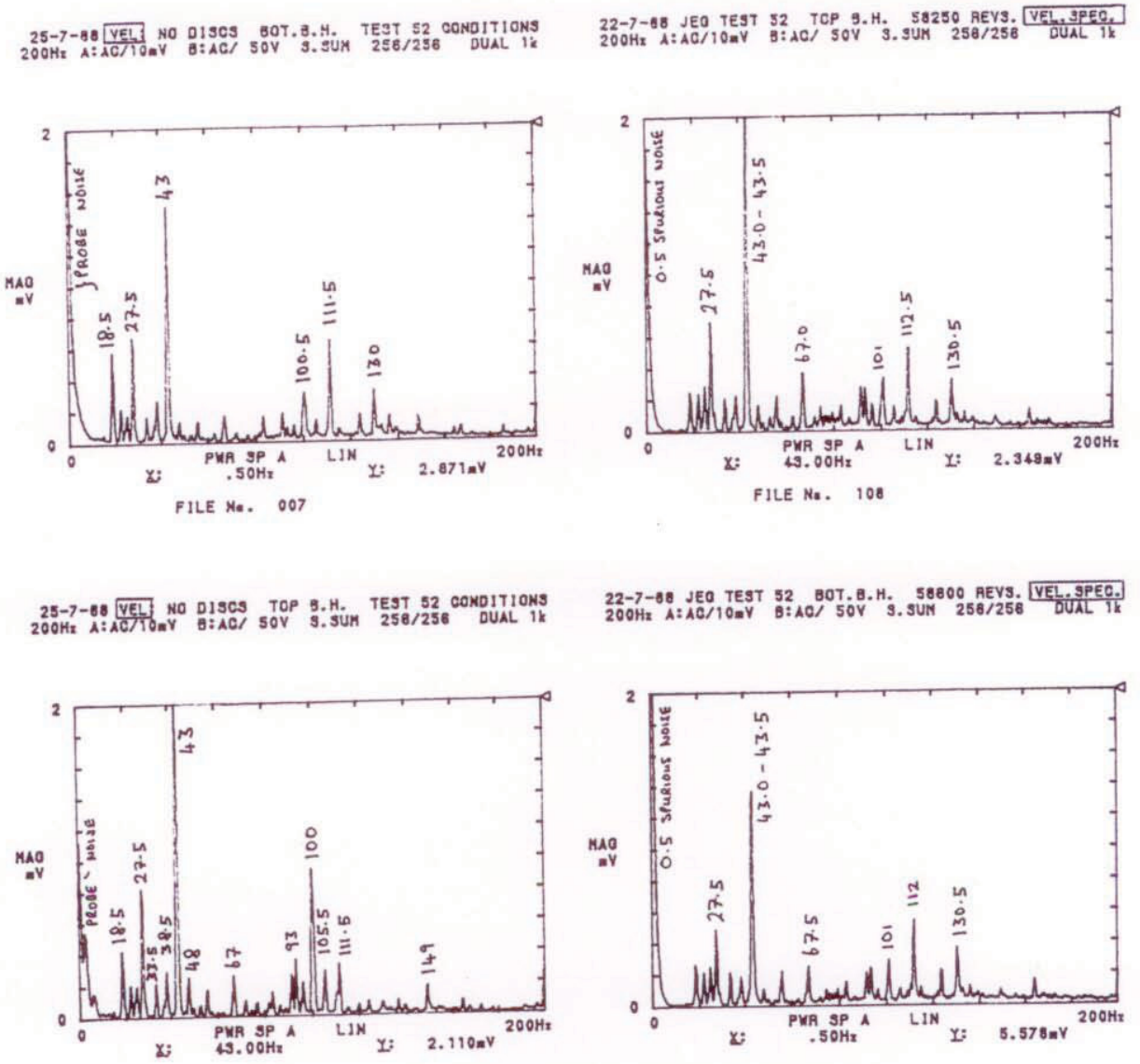

Figure 7.27 Comparative frequency spectra of velocities generated on LEROS with the machine running empty at low speed (leftside) and mid-way through the low speed test (Test 52, rightside), measured both on the top bearing housing (top figures) and bottom bearing housing (bottom figures).

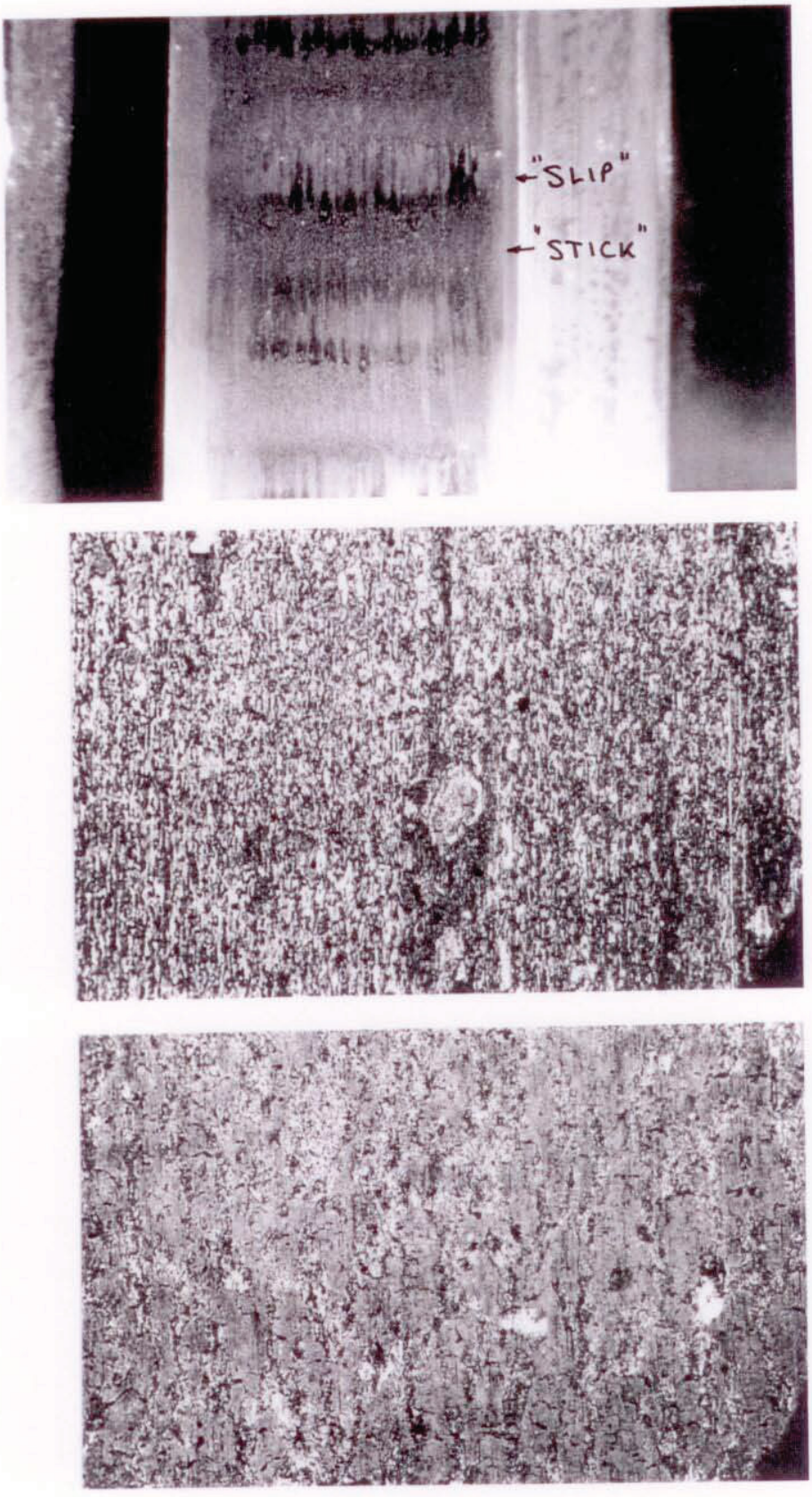

Figure 7.28 A LEROS (rail wheel) bottom disc taken from a water lubricated, rolling-sliding test (1500 MPa p_o, 1.35% creepage). (a) "Stick-slip" facet pattern on the oxidised surface (x5.3 mag.). (b) Close view of the "slip" area (x200 mag.). (c) Close view of "stick" area (x200 mag.).

CHAPTER 8

AMSLER and LEROS WEAR RESULTS

8.1 Introduction

Most of the test conditions were determined within the context of the research contract with British Rail and are representative of conditions on their rail network. As will be seen this has resulted in many results falling in a transitional zone of wear behaviour, between mild and severe wear. During some tests a change of wear regime occurred, marked by a sudden jump from one steady state wear curve to another. Previous British Rail work[Bolton et al, 1982; Bolton and Clayton, 1984] has examined wear with respect to the product of test conditions, $p_o\gamma$, where p_o is maximum contact stress and γ is circumferential creepage. This relationship is further examined in the Discussion (Chapter 10). For convenience, results in the present work have been grouped in $p_o\gamma$ order, however variations of stress or creepage within one value of $p_o\gamma$ gave quite different wear characteristics.

The test programmes for the modified Amsler and LEROS are given in Tables 6.1 and 7.1, respectively. Not all test conditions were duplicated on both machines, as test requirements changed as the research contract progressed and a requirement of LEROS was for tests under conditions which were beyond the capabilities of the Amsler machine. Where tests on both machines were at, or near, the same nominal levels of maximum contact stress and creepage, wear curves are presented in adjacent figures. Tabulated wear rate data are based on the least squares analyses of the linear parts of wear curves. Where a distinct change of wear regime has occurred during a test, two wear rates are presented ("Slopes A and B"). The effects of machine variables on wear rates, such as changes in the hydraulic loading system of the LEROS machine, are presented in these tabulated results.

8.2 Wear rate analysis

Initially, changes in air blast direction, the torque measuring system and disc grainflow orientations, plus the effects of differently spaced weighing intervals, were